SAND2012-9545P

Immune cell signaling: An integrated single-cell microfluidic analysis

By

MEIYE WU
B.A. (Oberlin College) 1997
M.A. (Boston University) 2001

Submitted in partial satisfaction of the requirements for the degree of

DOCTOR OF PHILOSOPHY

in

BIOCHEMISTRY AND MOLECULAR BIOLOGY

in the

OFFICE OF GRADUATE STUDIES

of the

UNIVERSITY OF CALIFORNIA

DAVIS

Approved:

_____

Kit S. Lam, M.D., Ph.D., Chair

_____

Charles Bevins, Ph.D.

_____

Paul Henderson, Ph.D.

Committee in Charge

2012

DEDICATION

This thesis is dedicated to my family – my husband Alan for his unwavering support, my son Alex for being the easiest, happiest baby ever, and my parents for their unconditional love. I couldn't have done it without you.

ACKNOWLEDGEMENTS

I would like to thank Dr. Kit S. Lam, Dr. Anup K. Singh, and Dr. Steve Branda for serving as my academic and corporate advisors, for guiding and supporting me through the completion of this body of work. Thanks to Dr. Chuck Bevins and Dr. Paul Henderson for serving on my qualifying and thesis committees. Thanks to Dr. Judy Kjelstrom and Marianne Hunter of the Special Degree Program for Corporate Employees at UC Davis, and to Catherine Culhane and Bernadette Montano of the University Part-Time program at Sandia, two programs that allowed me to pursue my degree without interruption to my career. Special thanks goes to Sandia colleagues Ron Renzi, Jim Brennan, Matthew Piccini, Dan Yee, and Dave Heredia for assistance in assembling the microfluidic platform, and also thanks to Dr. Aarthi Chandrasekaran and fellow Lam lab member Mary Saunders for insightful scientific discussion. Thanks to all the co-authors of my publications: Dr. Nimisha Srivastava, Dr. Thomas Perroud, Dr. Kamlesh Patel, Dr. Bryan Carson, Dr. Ken Sale, Dr. Cathy Branda, and Dr. Chung-yan Koh. Thanks to Dr. Urvashi Bhardwaj, the lab manager for Dr. Lam's lab for taking care of my administrative needs and for her expert management of the lab. Sandia is a multiprogram laboratory operated by Sandia Corporation, a Lockheed Martin Company, for the United States Department of Energy's National Nuclear Security Administration under contract DE-AC04-94AL85000.

ABSTRACT

Mammalian cell populations are heterogeneous and plastic in their response to stimuli and communication with each other. Multi-parameter quantitative experimental and computational methods that preserve single-cell resolution in these complex cell populations are necessary for elucidating the highly dynamic mechanisms that underlie cell signaling. This thesis explores various aspects of immune cell signaling using integrated microfluidic lab-on-a-chip technologies, capable of generating such multi-parameter single-cell measurements. A brief survey of existing single-cell resolution techniques and their applications in cell signaling studies, including microfluidic devices that evolved into those used in this thesis is discussed. Three microfluidic methods are developed for studying innate and adaptive immune cell signaling. The first method enables the spatiotemporal profiling of the toll-like receptor 4 (TLR4) pathway using a microfluidic device that seamlessly integrates cell culture, sample preparation, imaging and flow cytometry capabilities. Systems-level profiling of signaling proteins in the TLR4 pathway is performed in a single experiment on the integrated microfluidic platform, to generate data used for subsequent mathematical modeling. Next, a new single-cell resolution microfluidic method that combines metabolic labeling of bioorthogonal probes and proximity ligation assay to measure dynamically glycosylated proteins, a post-translational modification with widespread significance in cell signaling modulation, is demonstrated in T cells. The third method extends the utility of the microfluidic platform to measure microRNAs concurrently with proteins in intact T cells, to further expand the repertoire of signaling molecules that can be multiplexed and quantified at single-cell resolution. The lab-on-a-chip technologies developed in this

thesis present potential uses for several important applications including basic research, drug and biomarker discovery, biodefense, and for development of cost-effective point-of-care clinical diagnostics.

TABLE OF CONTENTS

LIST OF TABLES **Page**

LIST OF FIGURES **Page**

Chapter 1. Introduction

1.1 Variability within mammalian cell signaling networks

Heterogeneity of mammalian cell signaling networks has been widely recognized but only recently have tools become available that allow probing of genes and proteins in single cells to understand the stochastic behavior. While the advancement in single cell genomic analysis has been greatly aided by the power of amplification techniques (e.g., PCR), analysis of signaling proteins in single cells has proven to be more challenging. Numerous bioanalytical methods have been developed to analyze signaling proteins such as western blot, ELISA, immunoprecipitation and mass spectrometry. However, these methods require the availability of a large number of cells for assessment, resulting in a population-averaged measurement. Individual cells within a population can behave very differently, the behavior of some can be quite different from the average and this cell-to-cell variation has implications in various biological processes. For example, the heterogeneity in T cell populations underpin proper adaptive immune response, and has implications in clinical diagnostics as well as the development of novel therapeutics(*2, 3*). Other examples include stem cell differentiation(*4*) and analysis of circulating tumor cells (*5*). Therefore, measuring proteins (and other molecular signatures) at the resolution of single cells will greatly enhance our ability to understand molecular mechanisms of many cellular and disease processes (*6-8*).

1.2 Challenges in single cell protein analysis

The biggest challenges to measuring signaling proteins in single cells, assuming single cells have been successfully isolated from a tissue, or culture, are the minute amount of protein present and the enormous complexity of the proteome. Adapting

traditional bulk protein analysis methods for single-cell level applications has met with varied degrees of success, with quantitative analysis being especially elusive. Proteomic measurements can be quite complex as there are various types of measurements to be made – protein abundance or expression levels, post-translational modifications (especially phosphorylation and glycosylation), protein translocation, protein interactions with other proteins, DNA etc., and protein activity (Figure 1.1). No one analytical method can be used to study all these in single cells, so a suite of biochemical and biophysical methods have been developed. Protein concentrations and post-translational modifications are best assessed using mass spectrometry and flow cytometry; protein localization and dynamics is effectively studied using microscopy; protein/protein interactions can be characterized using microscopy techniques such as fluorescence resonance energy transfer or fluorescence correlation spectroscopy; and protein activity can be measured by fluorescent spectroscopy.

1.3 Single-cell protein analysis by flow cytometry

The most established and user-friendly method for signaling protein analysis is flow cytometry. Its effectiveness derives from the fact that while the absolute protein amounts in a cell can be vanishingly small, the localized protein concentrations can be larger and measurable if the cells are kept intact. Flow cytometry, since its invention in the late sixties, has been transformed from a technique limited to measuring 1-2 fluorescent species in a cell to 10-15 today allowing profiling of entire pathways in single cells. This has been enabled by advancements in both instrumentation and availability of highly specific antibodies. Fluorescence-activated cell sorter with 3-4

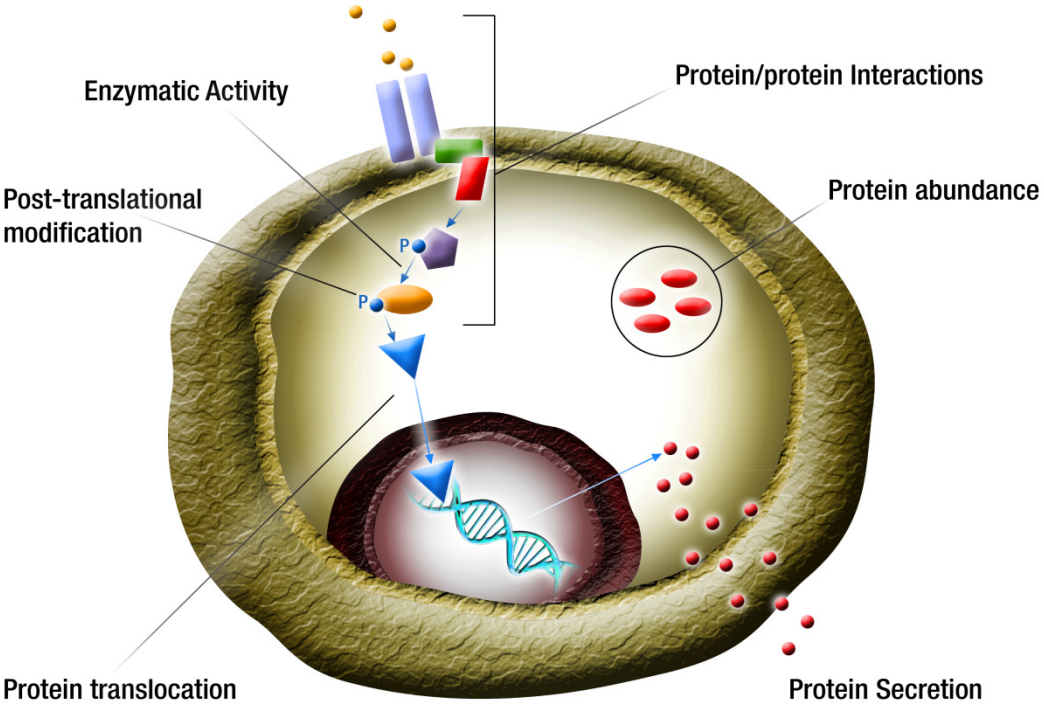

Figure 1.1 Mammalian cell signaling network is complex and requires measurements of many attributes including abundance or concentration of cytosolic, membrane-bound and secreted proteins, protein interactions with other proteins and molecules, inter- and intra-organelle translocation of proteins, post-translational modifications, and enzymatic and other activities of a protein. Colored shapes represent different proteins. P – phosphorylation.

lasers allowing resolution of up to 16 organic dyes or quantum dots are available from multiple companies. Similarly, high-quality antibodies have become commercially available to selectively label important proteins and protein modifications in cells. DeRosa (*9*) (*10*), and Nolan (*11*) groups pioneered the use of multi-parameter analysis using multi-color flow cytometers to measure 10-15 key proteins in signaling pathways simultaneously in single cells. The ability to perform correlated measurements of multiple proteins in single cells has turned cytometry into a powerful tool for semi-quantitatively analyzing pathways underlying many diseases (*12, 13*).

Flow cytometry can also be used for analysis of proteins such as cytokines that are normally secreted. This requires treating cells with a vesicle formation inhibitor to trap synthesized cytokines in the Golgi, followed by fixation and permeabilization to stain the trapped cytokines with fluorescent mAbs for flow cytometric analysis(*14*). One shortfall of traditional flow cytometry is the inability to determine the intracellular localization of proteins. To this end, imaging cytometers have been developed to provide both localization and signal intensity information(*15*). However, the throughput of imaging cytometers is greatly reduced when compared to the flow cytometer, making it cumbersome for certain applications.

1.4 Microfluidic flow cytomtery for signaling protein analysis

While commercial flow cytometers allow interrogation of cells one at a time, the sample preparation is still done manually, and therefore requires a large numbers of

cells to compensate for sample loss during preparation. This makes it hard to analyze samples that are limited in volume such as cells recovered from a biopsy sample, tissue specimens or small volumes of blood. To permit analysis of small number of cells (100-1000), microfluidic platforms have been developed that integrate sample handling with flow cytometry (*16*). Srivastava et. al. (*17*) developed an integrated microfluidic device, retro-fitted to commercial microscopes, that can perform cell culture, stimulation and sample preparation in combination with conventional fluorescence imaging and microfluidic flow cytometry (Figure 1.2, 1.3) to monitor immune response pathways in macrophages. The microfluidic device not only drastically reduced the amount of sample and reagent required, it also provided a means to perform two orthogonal modes of measurements, imaging and cytometry, in one experiment. The work done in this thesis aims to incrementally improve upon this platform, and find more applications for single cell resolution analysis on the improved microfluidic chip platform.

1.5 Microfluidic platform improvements

One of the objectives of this project is to improve the multiplexing capability of the microfluidic platform developed by our group previously(*17*). Only two experimental conditions were allowable on the first generation platform, which is not enough throughput for any realistic biological study (figure 1.4.A). As the microfluidic assays became more sophisticated, it was necessary to upgrade the throughput of the chip to be compatible with biologically relevant problems. A series of new chip designs were fabricated and tested. First, a four-chamber chip was tested and used to

generate data for pathway profiling studies outlined in chapter 2 (figure 1.4.B). Then, newer chip designs with even higher throughput was tested (figure 1.4.C, D). The 6

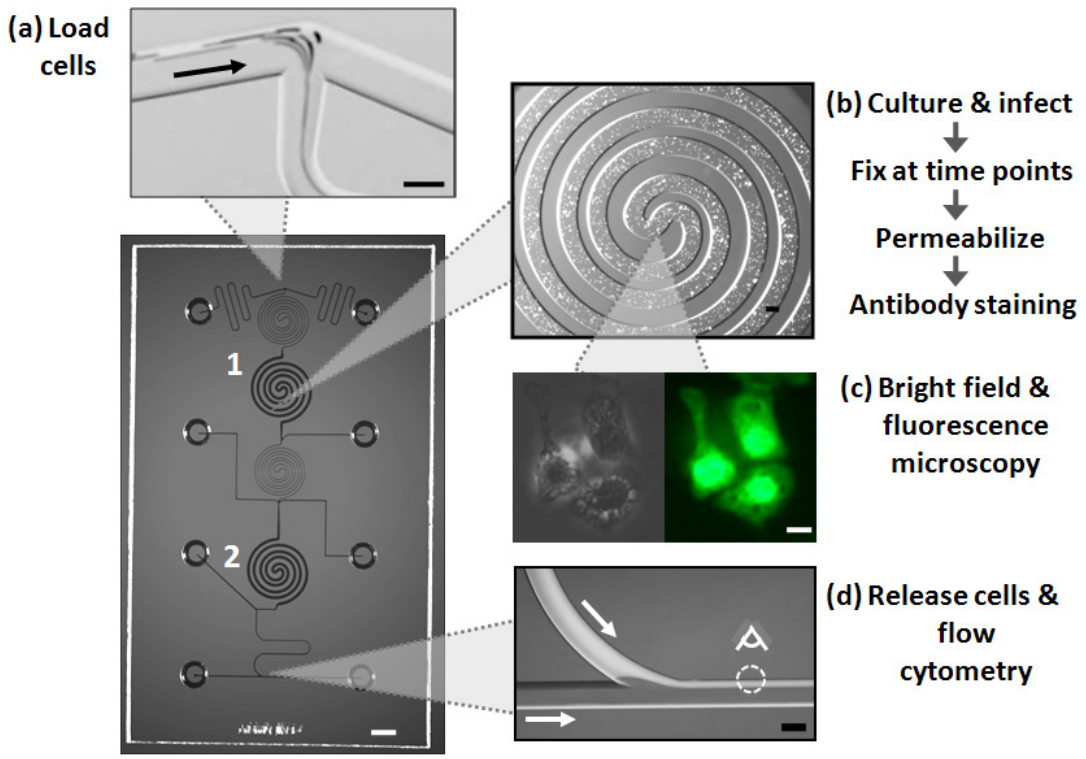

Figure 1.2 Microfluidic Platform for single cell resolution analysis. An integrated microfluidic platform that integrates cell culture and sample preparation with two orthogonal single-cell resolution techniques- flow cytomtery and fluorescence microscopy(*17*).

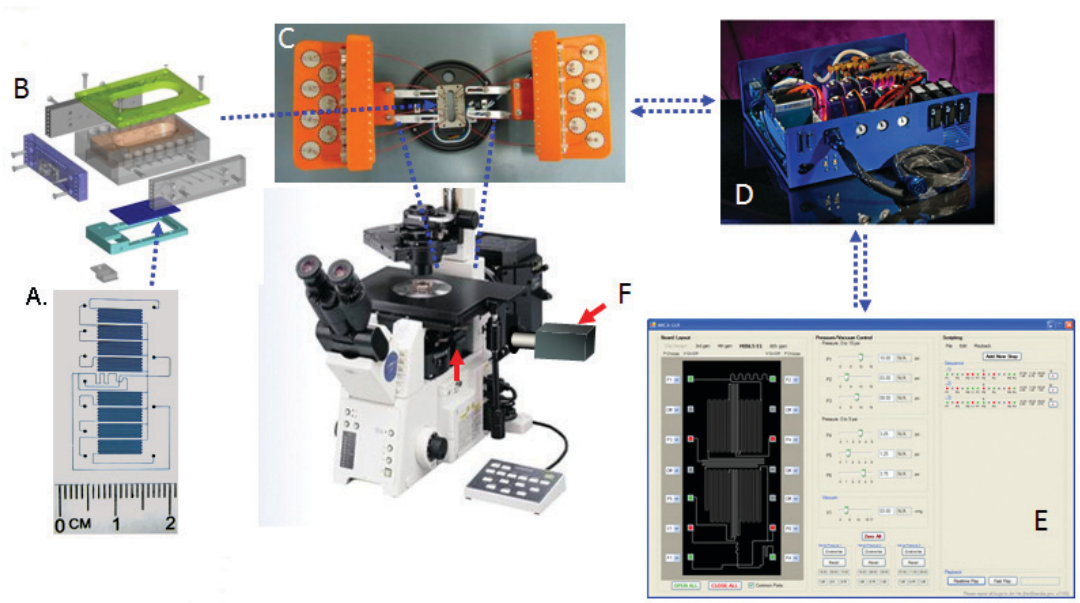

A	Monolithic microfluidic quartz chip
B	Thermo-regulated 14-port manifold
C	14-valves interface and thermo-regulated reservoir bank
D	System controller with umbilical link
E	Programmable graphic user interface for automation
F	Flow cytometer module – 2 lasers (488 nm and 635 nm) and 5 detection channels (scattering + GFP, YFP, Cy5, Cy7 fluorescence)

Figure 1.3 Integrated microfluidic platform for cell signaling analysis. The premixed 5% CO2 is directly plumbed into the valve setup shown in C. The temperature controller (not shown) connects the chip and manifold (A&B) to the system controller (D). The graphic user interface (E) allows for user programming and hands-free operation of the entire experiment from dosing to sample preparation, to analysis.

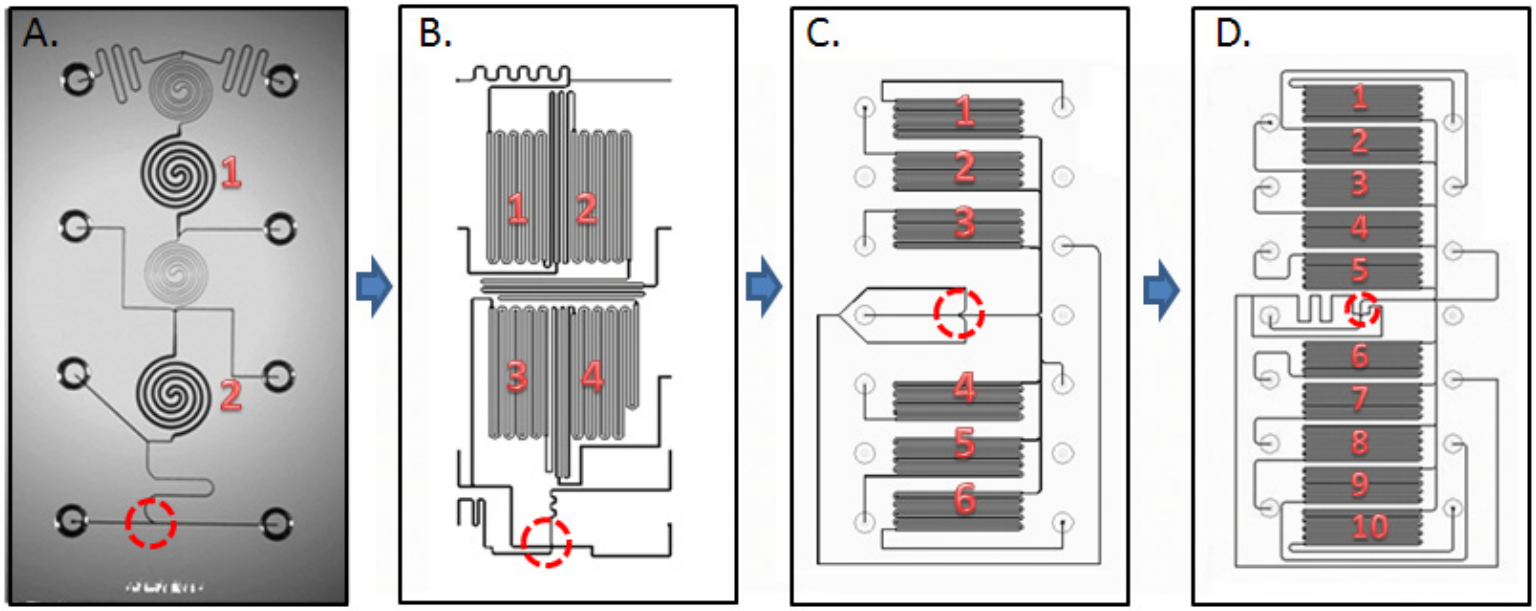

Figure 1.4 Four generations of microfluidic chip designs to improve the throughput and operation of single-cell resolution studies. The fluidically isolatable cell holding chambers are numbered in red, and the point of on-chip flow cytometry detection are marked with red dash circle. The first generation chip shown in (A) was used for detecting singular protein phosphorylation, with only one experimental and one control condition allowed per experiment. The second generation chip shown in (B) has double the number of cell holding chambers and two sheath channels for better hydrodynamic focusing. Third and fourth generation chips have even higher throughput and detection point moved to the center of the chip to minimize cross contamination between chambers.

chamber designs proved very useful in the subsequent bioorthogonal labeling of glycoprotein experiments presented in chapter 3, and the 10 chamber chip was used for chapter 4's microRNA florescent *in situ* hydridization experiments. Aside from the improved throughput, the new chip designs (figure 1.4 B, C, D) all use two sheath streams for better hydrodynamic focusing at the point of on-chip flow cytometry, and the 6 and 10 chamber chips are designed so that cells from each chamber can directly travel to the flow cytometry detection point at the center of the chip without having to travel through other chambers. The direct path to flow cytometry detection point eliminated cross-contamination between chambers. Premixed CO_2 plumbed directly into the pressure controller allowed long term cell culture in the chip, and was used to study cytokine release and live cell imaging in the pathway profiling experiments presented in chapter 2. Overall the engineering improvements made to the microfluidic platform enables the study of a wider variety of signaling events in one experiment, providing systems level data acquisition capability.

1.6 Labeling and flow cytometric analysis of signaling glycoproteins

While flow cytometry has been most commonly used for analysis of kinases and phosphatases, it is easily applicable to analysis of other enzymes and protein modifications. For example, glycosylation in single cells can also be profiled using labeled lectins and flow cytometry. Venable et al. used a panel of 14 lectins to characterize glycans present on cell surface as potential markers of pluripotency in human embryonic stem cells(*18*). A factor limiting the wider application of flow cytometry to glycolsylated protein is that there are very few lectins available. A

promising development has been introduction of selective bioorthogonal chemical probes for metabolic labeling of glycans (*19*). This strategy involves incorporation of unnatural chemical reactive groups into cellular glycans (by metabolic labeling) followed by fluorescent(*20*) or bioluminescent(*21*) labeling of the reactive groups. So far, these bioorthogonal glycan probes have been used in imaging studies, but they should be useful for flow cytometry-based detection of glycosylation. To pioneer the use of bioorthogonal labeling for flow cytometry, we developed a method that combined bioorthogonal labeling and proximity ligation assay was developed to detect glycolsylated proteins on the microfluidic platform, and the results are presented in chapter 3.

1.7 Detecting microRNA in cell signaling using microfluidic flow cytometry

Cell signaling networks comprise of more than just protein. Recent discovery of micro RNAs (miRNAs) have revealed that small, non-coding RNAs can "fine tune" cell signaling responses by post-transcriptionally controlling the expression level of signaling proteins(*22*). By controlling the translating of mRNA targets, miRNAs may occupy a unique role in the dynamics of cell signaling networks. First, miRNAs act in a shorter time scale than protein transcriptional repressors because miRNAs are processed more quickly than protein transcription factors, as they do not require translation and retrotransport to the nucleus. Second, since miRNAs act at the RNA level, they act slower than post-translationally activated enzymatic proteins such as kinases that can directly inhibit its targets. Hence, miRNAs can act as early initiators of gene regulation in certain contexts such as miR155 in innate immune response(*23*),

where fast response to pathogen is crucial, but also act as a "delay switch" in negative feedback regulation of immune response at a later time scale to dampen the response(*24*).

Several methods exist for the detection of miRNAs. Most miRNA detection methods such as Northern blotting(*25*), oligonucleotide microarrays(*26, 27*), qPCR-based detection miRNAs(*28, 29*), and next generation sequencing(*30*) all require the homogenization of large number of cells and making an averaged miRNA measurement. Population averaged miRNA measurements obscure cell to cell variation and population-specific miRNA differences that are known to be important for miRNA function. In addition, none of the population-based detection methods provide capability to multiplex protein analysis with miRNA detection. To address this need, a microfluidic based method for detecting miRNAs and proteins in the same intact cell was developed using locked nucleic acid probes, and presented in chapter 4. The novel method holds promise of better detection and analysis of miRNAs in their native environment for better understanding of their function and use as biomarkers for disease.

Chapter 2.

Microfluidically-unified cell culture, sample preparation, imaging and flow cytometry for measurement of cell signaling pathways with single cell resolution

2.1. Abstract

We have developed a microfluidic platform that enables, in one experiment, monitoring of signaling events spanning multiple time-scales and cellular locations through seamless integration of cell culture, stimulation and preparation with downstream analysis. A combination of two single-cell resolution techniques-- on-chip multi-color flow cytometry and fluorescence imaging provides multiplexed and orthogonal data on cellular events. Automated, microfluidic operation allows quantitatively- and temporally-precise dosing leading to fine time-resolution and improved reproducibility of measurements. The platform was used to profile the toll-like receptor (TLR4) pathway in macrophages challenged with lipopolysaccharide (LPS) - beginning with TLR4 receptor activation by LPS, through intracellular MAPK signaling, RelA/p65 translocation in real time, to TNF-α cytokine production, all in one small macrophage population (<5000 cells) while using minute reagent volume (540nL/condition). The platform is easily adaptable to many cell types including primary cells and provides a generic platform for profiling cellular processes.

2.2. Introduction

The response of mammalian cells to stimuli is highly dynamic and complex. Typically, cellular response manifests as a cascade of signaling events that cross multiple cellular locations and timescales. To properly understand cell signaling pathways, multiple signaling events must be measured simultaneously in order to establish precise spatiotemporal correlations(*31*). Multiplexed analysis of cellular signaling can be extremely challenging, however, as it requires measurement of categorically different types of signaling events (e.g., protein translocation vs. post-translational modification) that occur in different subcellular compartments (e.g., nucleus vs. cytosol) and at different timescales (e.g., receptor activation within seconds vs. protein expression over hours). To monitor these diverse processes, numerous stand-alone techniques-Western blot analysis(*32*), enzyme-linked immunosorbant assay (ELISA) (*33*), microarrays (*34*), live-cell imaging(*35*), and flow cytometry(*36*), each with its own sample preparation requirement, are used to acquire data at various stages of signaling. Performing each type of analysis independently obliterates the spatiotemporal relationship between each signaling event, and also introduces significant experiment-to-experiment variability. Furthermore, many of the traditional techniques, such as microarrays, Western blots, microarrays and ELISA require a large number of cells and provide only population-averaged data. Cells are heterogeneous in nature and hence, population-averaged data can be misleading; therefore, data obtained at single-cell resolution would be more desirable (*37, 38*). For example, dynamic response of tumor suppressor protein p53 network derived from population studies was found to be misleading as individual

cells showed series of undamped p53 pulses with fixed amplitude and duration rather than damped oscillations seen in population-averaged data(*39*). Similarly, real-time imaging of transcription factor RelA translocation in single cells revealed variability in the oscillatory dynamics of RelA translocation among single cells, and that RelA translocation dynamics determined the degree and timing of downstream gene expression(*40*).

To overcome the limitations of conventional methods, one would like to have experimental platforms capable of measuring dynamic response of an entire pathway in a single experiment, one cell at a time. Owing to their advantages in integration and multiplexing, microfluidic platforms have attracted significant attention in cellular analysis(*41*). Microfluidic platforms have been developed for many unit functions such as cell culture(*42-44*), flow cytometry(*45-49*), cell sorting(*50-52*) and single cell imaging(*53-56*). We recently reported on chip-based flow cytometry for measurement of genes (by fluorescence *in situ* hybridization)(*57*) and proteins (by immunostaining) in single cells(*17*). However, the approaches described to date are focused mostly on individual signaling events (phosphorylation of one protein) and do not integrate the multiple steps required to comprehensively and quantitatively interrogate serial events in cellular pathways using both biophysical (live-cell imaging) and biochemical (flow cytometry) measurements.

Building upon our previously reported devices for cytometry(*50, 57*) and singular intracellular phosphorylation assays(*17*), we report development of a microfluidic platform that enables, in one experiment, monitoring of signaling events spanning multiple time-scales and cellular locations, through seamless integration of cell

culture, stimulation, and preparation with downstream analyses. Two single-cell resolution techniques – multi-color flow cytometry and fluorescence microscopy – are used in combination for multiplexed and orthogonal analyses. The platform is capable of making categorically different types of measurements (e.g., translocation of a transcription factor and phosphorylation of a kinase) in one platform enabling correlations among events. This is crucial for quantitative understanding of global cell dynamics. Moreover, it is capable of measuring kinetics with unsurpassed resolution (~s) and a wide dynamic range (~s to ~h) allowing measurements of both early and late events. The platform also integrates and automates numerous time-consuming and labor-intensive steps, thereby significantly reducing experimental variability.

The TLR4 (toll-like receptor 4) pathway in macrophages serves as our model pathway, due to its proven clinical relevance as part of the innate immune response to bacterial infection(*58-62*) and abundant existing commercially available antibody repertoire. The TLR4/MD2 receptor complex recognizes the bacterial cell surface component lipopolysaccharide (LPS) on gram-negative bacteria(*63, 64*). Upon binding to LPS, the TLR4 receptor undergoes conformational change that leads to dimerization (*65, 66*), followed by signaling via MyD88-dependent pathway which culminates in the activation of MAP kinases(*67*) and RelA/NFkB translocation into the nucleus to induce the expression of proinflammatory cytokines including TNF-α, IL6, IL8, IL16,(*68*), along with other mediators that control the growth and spread of invading bacteria(*69-71*). Based on the existing TLR4 pathway model (*72-74*), we divided the TLR4 response into four general levels: TLR4 receptor activation, intracellular phosphorylation, RelA translocation, and cytokine production (Fig.2.1A).

In this study, we perform temporal dissection of each node using our platform, followed by the profiling of all four levels of the TLR4 signaling cascade in one chip experiment. All protein nodes and fluorephores used in this study are outlined in table 1.

Level in TLR4 pathway	Time	Method	Protein Target	Fluorophore	Excitation (nm)	Emission (nm)
TLR4 receptor activation	0s, 30s, 30m	Microscopy, flow cytometry	TLR4/MD2 complex	PE	488	585/42
Intracellular MAPK phosphorylation	0s, 30m	Microscopy, flow cytometry	Phospho-ERK 1/2	Alexa-647	635	670/20
RelA-GFP translocation	0s to 2h continuous	Time-Lapse Microscopy	RelA(P65)	GFP	488	530/30
Cytokine Production	0h, 4h	Microscopy, flow cytometry	TNF-α	Cy5	635	660/20

Table 1. The protein targets and fluorephores used in the pathway profiling experiment represented in figure 2.9.

2.3. Materials and Methods

RelA-GFP stable macrophage cell line generation and maintenance

The RAW 264.7 murine macrophage cell line was purchased from ATCC (Manassas,VA) and was used to generate the RelA-p65-GFP stable cell line. The pActin-EGFP-RelA construct was derived from pECFP-F-RelA, a kind gift from Dr. Allan R. Brasier (University of Texas Medical Branch,Galveston, TX). Transfection of RAW cells were done using the Amaxa nucleofection system according to manufacturer's instructions(VCA-1003, Lonza) The stably transfected RAW 264.7 Macrophages were cultured in growth medium consisting of 450 mL of DMEM, 50 mL of FBS (Gemcell), 10 mL of HEPES, 5 mL of L-glutamine (200 mM), and 1:100 penicillin/streptomycin (Gibco) and 200ug/mL Geneticin (Invivogen).

Microfluidic assay platform design and assembly

The four chamber microfluidic chip was designed in-house using AutoCAD 2000 (Autodesk Inc., San Rafael, CA), photomasks were generated at Photo Sciences (Torrence, CA), and quartz microfluidic devices were fabricated by Caliper Life Sciences (Hopkinton, MA). An array of fourteen holes (500 μm diameter), seven on each side, provided for fluid inlet. Fluidic connection to the inlet holes was made using an in-house designed plastic (delrin) manifold and PEEK tubing (125 μm ID, 1/32 in OD, Upchurch Scientific). An in-house designed shutoff electronic valve (response time < 1 s, dead volume ~20 nL) was used inline with the PEEK tubing. On the other end, the PEEK tubing was immersed in an airtight sample/reagent reservoir.

The reservoir was pressurized using 5% pre-mixed CO_2 and electronic pressure controllers (Parker Hanifin, Cleveland OH) in order to load sample/reagent into the chip. Pressures ranging from 0.2 to 5 psi were used during cell signaling assays. Finally, the microfluidic channels as well as the inlet holes were completely filled with DI water before the fluidic connections were assembled. The chip is reusable (>100 experiments) and can be cleaned using common disinfectants (bleach, ethanol, or detergents). The thermal control setup was mounted on the chip platform to achieve the desired temperature regulation during cell culture and stimulation. The thermal control setup consisted of a thermoelectric hot plate (TE Technology Inc., Traverse City, MI) and a proportional integral controller. A temperature sensing thermistor was attached to the quartz chip to provide temperature feedback to the controller. The setup was capable of maintaining temperatures from 0 to 100 °C with an accuracy of ±0.1 °C. For CO_2 maintenance during the course of the experiment, a pre-mixed 5% CO2 and 95% air cylinder (Tri-Valley Gas, Livermore, CA) was plumbed into the system to supply the air pressure for flowing reagents and media onto the chip.

Cell surface and Intracellular Immunostaining and time lapse imaging

The planar microfluidic cell preparation chip in this study contains four vertical fluidically isolatable microchannel series with the dimensions of w = 260 μm width, d = 35 μm depth, L = 72 mm, each holding up to 3000 macrophages and 540 nL of fluid volume. The four-chambered microfluidic chip was coupled to fluid control hardware containing series of pumps and valves controlled by via software graphic user interface with programming capability. Macrophage suspension of 2×10^7 cells/mL

was loaded into the chambers and allowed to adhere for 5min without flow. Conditioned media containing 100 nM *E. Coli* smooth LPS (L4524, Sigma-Aldirch) was flown into holding chambers 1, 2 and 3 at a velocity of 1400 nL/min, measured with a Upchurch flow meter, starting at t_0 and lasting for 30 s to 4 h. t_0 was defined as the time at which the LPS fluid boundary arrives at the midpoint of the cell holding channel. Conditioned media without LPS was flown into a neighboring cell chamber for the duration of the LPS challenge to serve as control. Macrophages were fixed with 1.5% paraformaldehyde for 10m, permeabilized with a PBS based solution containing 0.1% Triton and 0.05% CHAPS for 20 min, and stained with fluorescent labeled antibodies targeting TLR4/MD2 surface receptors(117605; Biolegend), intracellular phospho-specific ERK1/2(4375; Cell Signaling), and intracellular TNF-α(19-7321-81, eBiosciences) for 30 min. One chamber of the chip was used for both real-time imaging of RelA-GFP translocation and intracellular TNF-α immunostaining. After 2 hours of real-time imaging, 1μl/ml of Golgi-Plug reagent containing Brafeldin A (555029; BD Biosciences) was introduced into the chamber for 2 hours prior to immunostaining. Two hours of Brefeldin A treatment did not alter ERK and TLR4/MD2 baseline fluorescence (data not shown). Bright field, epi-fluorescence and phase contrast images were captured at 60X and 100X magnification on an Olympus IX-71 inverted microscope equipped with a CoolSNAP HQ CCD camera (Photometrics, Tucson, AZ) and Image-Pro software (Media Cybernetics, Bethesda, MD). The fluorescent time-lapse imaging was acquired using an automatic shutter (Sutter Instruments) controlled through Image-Pro software.

On-chip Flow Cytometry

For all on-chip flow cytometry experiments, measurements were performed on a modified two-stage inverted microscope (TE-2000U; Nikon Instruments, Melville, NY) similar to that described previously,(*50*) with the following modifications. A 20-mW 488-nm solid-state laser (Cyan; Newport, Irvine, CA) and a 20-mW 635-nm solid-state laser (FCLM635; OPLink, Fremont, CA) are coupled to the back of the microscope using a cylindrical lens (Thorlabs, Newton, NJ), which focuses the two laser beams at the back-aperture of a 40X 0.6 N.A. microscope objective (Plan Fluor ELWD; Nikon Instruments). Forward scattering of the blue laser is detected through an optical fiber (JTFSH 600 μm core; Polymicro Technologies, Phoenix, AZ) and a bandpass filter with blocker (488NB2.6; Omega, Brattleboro, VT) connected to a photomultiplier (H5784-20; Hamamatsu, Bridgewater, NJ). Forward scattering of the red laser is detected through the same fiber using a bandpass filter with blocker. Laser-induced fluorescence emission is split (600DCXR longpass filter; Chroma, Rockingham, VT) into a yellow channel (FL2-H: 585/42m bandpass filter), and following a second dichroic (750DCXR longpass filter; Chroma) into a red channel (FL3-H: 655LP longpass filter) and a far-red channel (FL4-H) before being detected by three photomultipliers. All five photomultiplier voltages (488-nm scatter, 635-nm scatter, yellow, red and far-red) are recorded by a data acquisition module (NI 9401; National Instruments, Austin, TX). After on-chip sample preparation, cells were detached via proteolytic cleavage using 100ug/mL elastase (I.U.B.: 3.4.21.36,Worthington), and hydrodynamically focused for on-chip flow cytometry. The focusing is in one plane and the flow is focused in the center of the channel using

sheath flow from two sides. There is no focusing in the vertical (or, radial) direction. The sheath channels and the sample channel have the same depth (35 μm) and the sample stream is focused in a rectangular cross-section 20 μm wide and 35μm deep, which is entirely contained within the laser beam path at the point of detection. In-house software for data collection was scripted using LabVIEW. The scatter and fluorescence captured by each PMT module was collected using a computer equipped with National Instruments data acquisition module, and the data was further analyzed using the Peak Finder application in LabVIEW. The Peak Finder application fit the peak of the raw voltage signals from the PMT with a polynomial fit, generating the peak amplitude and width values. The text files containing peak values for each scatter and fluorescence measurement were then imported into Microsoft Excel, and histograms for each experimental condition were generated and overlaid using Excel.

Western Blot Analysis

RAW264.7 cells were seeded 24 hours prior to experiment on 10cm tissue culture plates (BD 35305) at a density of 3×10^6 cells / dish. On the day of the experiment, 1 ml of 10X LPS stock diluted in growth media were added to designated plates for predetermined periods of time. At time of harvest, the supernatant was harvested and stored at -80°C for TNF-α ELISA assays. The adherent cells were then harvested by incubating with 1 ml of sample buffer containing SDS and β-mercaptoethanol for 5min at room temperature, and scraped with a cell lifter (Corning No.3008). Harvested cells were stored at -80 °C until Western Blotting analysis was performed. 10ul of each sample was run on Novex 4-20% Tris-Glycine Midi gel (Invitrogen, WT4203BOX), at 150V for 90m. Transfer was done on the iBlot transfer system

(Invitrogen IB1001) for 7:00min. The PVDF membrane was blocked in 15 ml of blocking buffer (5% dry milk in TBS/T) for 1 hour at room temperature and washed 3 times with TBS/T. The PVDF membrane was incubated with primary antibody phospho- p42/44 MAPK (Cell Signaling 4377s), in 5% BSA (Sigma 3803) in TBS/T at 4°C overnight with gentle agitation. The following day, the membrane was washed 3 times with TBS/T and incubated with HRP-conjugated secondary antibody (GE Healthcare) in 5% dry milk in TBS/T for 2 hours at room temperature, followed by 3 washes in TBS/T. Protein abundance was detected using ChemiGlow reagent (AlphaInnotech 60-12597-00) on the AlphaImager from AlphaInnotech.

TNF-α ELISA assay

RAW supernatants were diluted 1:10 and tested with the Quantikine mouse TNF-α kit (MTA100) from R&D Systems according to manufacturer's instructions.

2.4. Results and Discussion

TLR4 signaling occurs at multiple time-scales and locations: receptor activation (at cell membrane, ~s), protein modifications such as phosphorylation (in cytoplasm, ~min), translocation of transcription factors (from cytoplasm to nucleus, ~min-h), and protein expression and secretion (~h) (Fig. 2.1A). We used the chip platform to first dissect the kinetics of each time-scale, followed by the profiling of the entire pathway in one chip and in one experiment. Immunostaining combined with on-chip multi-parameter flow cytometry was used to quantitatively measure receptor activation, protein modification and expression (Fig.2.1B). Fluorescent imaging of the immunostained cells was used to verify the cytometry results. Stable cell lines carrying green fluorescent protein (GFP) tagged to a transcription factor were created to observe translocation in real-time by microscopy. Microscopy was also used to track the location and health of cells.

The microfluidic platform consists of a chip with four fluidically-isolatable cell holding chambers (Fig. 2.1.C) designed to accommodate four parallel experiments, fitted in a manifold and valve setup. The chip is made out of glass, and its 150μm-thick bottom surface allows high-resolution imaging using an inverted microscope (Fig. 2.1.D). Cells suspended in growth medium are loaded into the chip's reservoirs and then delivered into the holding chambers; flow is stopped briefly to allow the cells to settle and adhere to functionalized bottom surface. Reagent addition and removal, and cell washing, are performed using pressure-driven flow. The rapid fluid exchange and mixing enabled by computer-controlled valves, together with the microscale dimensions of the chip, enable the researcher to change the cells'

environment with temporal precision (~s) that cannot be achieved in macroscale assays. Upon release from the holding chambers, cells are focused into a single-file line through two-dimensional sheath flow, and are interrogated individually by a five-channel (2 scattering, 3 fluorescence) detector (Fig.2.1E). The four independent reaction chambers and three-color detector provide the ability to multiplex up to four assays in one experiment. Details of the chip operation for on-chip immunostaining is illustrated in figure 2.2, and details of chip operation for on-chip flow cytometry is illustrated in figure 2.3.

The chip is compatible with both adherent and non-adherent cell lines and primary cells. We have successfully cultured adherent cells including murine macrophages (RAW 264.7, J774.1, P388D.1), mast cells, human epithelial cells, and non-adherent cells such as primary human peripheral blood mononuclear cells. Constant perfusion with CO_2-perfused media and precise temperature control keep the cells viable for 24-48 hours (Fig. 2.4) allowing ample time to complete cell signaling experiments. Chips can be coated with covalent (*via* silane chemistry) and non-covalent coatings (*e.g.*, fibronectin, collagen, Cell-Tak) to encourage cell attachment during culturing and/or cell preparation.

A concern in any perfusion system for cell culture is whether cells are perturbed by the flow or shear stress. At 1400 nL/m measured flow rate, the cells inside the microchannel experiences approximately 30 dyne/cm^2 comparable to shear experienced during routine pipeting of cells and reagents. The highest flow rates used neither detached macrophages from the glass surface nor were substantial enough to

activate the cells as previously reported(*17*) by monitoring activation of a shear stress sensitive kinase MAPK.

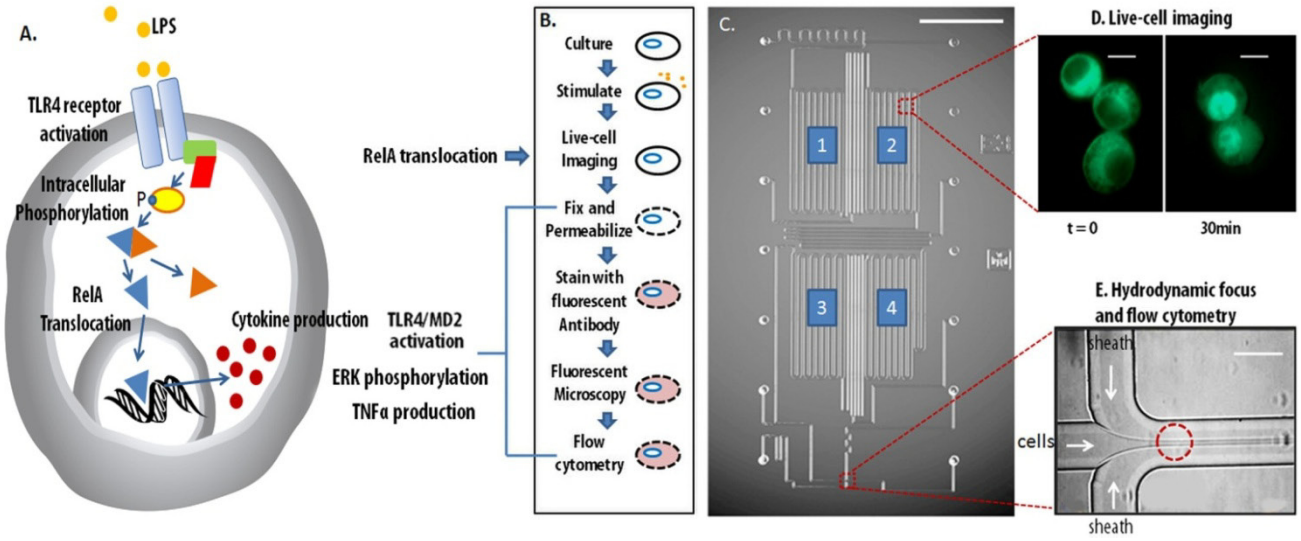

Figure 2.1. A microfluidic chip for global profiling of cellular pathways. TLR4 signalling events occur at different timescales and subcellular locations (cell diagram shown in A). Panel B shows all procedures that are integrated and performed on the chip shown in C. All the representative events in the cell diagram (A) can be profiled using both fluorescent microscopy (D) and flow cytometry (E). Real-time imaging of cellular response can be monitored by live cell fluorescent microscopy (D, scale bar = 10 μm), and after which, immunohistochemistry of other proteins are performed. Cells are then released via enzymatic cleavage, and focused into a single-file line through two-dimensional sheath flow (E), and passed through a laser detection point (Red circle), and interrogated individually by a five-channel (2 scattering, 3 fluorescence) detector.

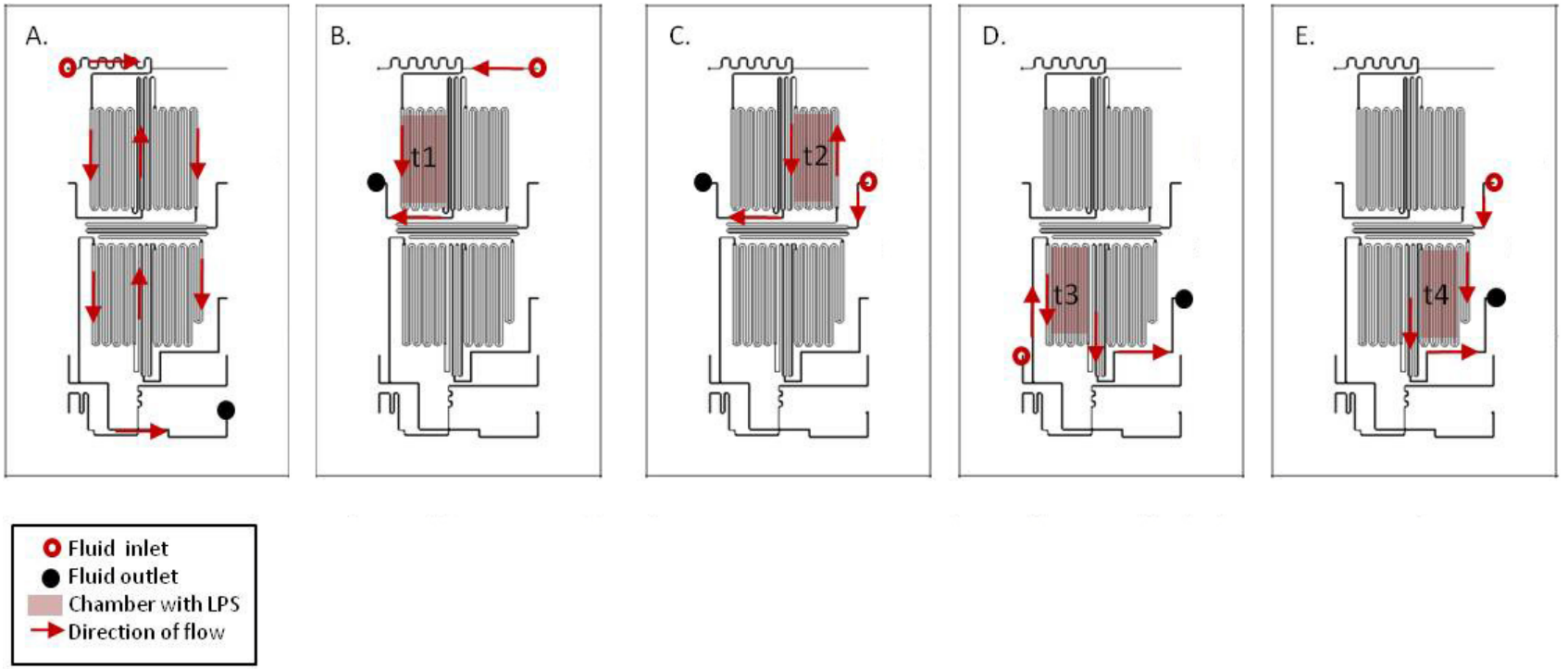

Figure 2.2 Operation of the 4-chamber chip for sample preparation. To perform the time course experiments, cells were driven into the chip by positive pressure from a port at the top of the chip (red circle) to the bottom (filled black circle), populating all 4 chambers. (A). Each chamber can be fluidically isolated and incubated with media containing LPS (B-E). for predetermined amounts of time. Cells in each chamber were then fixed by flowing 1.5% paraformaldehyde in PBS for 10 min, and all subsequent steps in sample preparation was done by flowing reagents from top left port to bottom right port as shown in A.

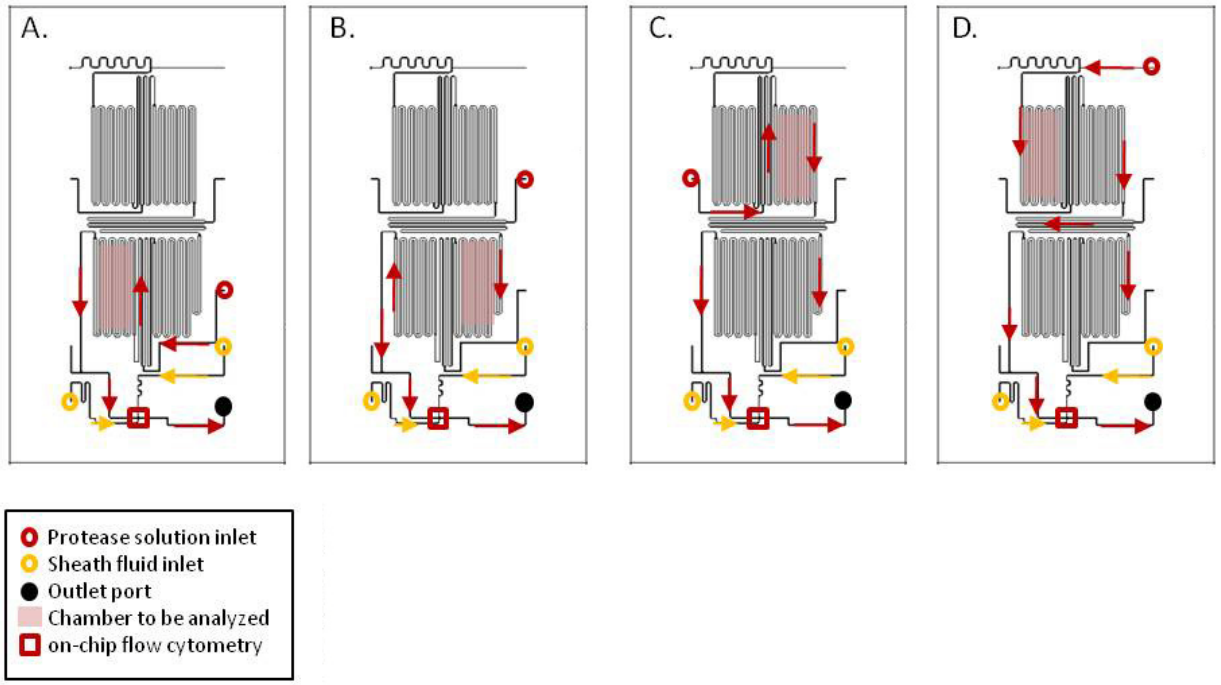

Figure 2.3 Device operation for on-chip flow cytometry. After stimulation, fixation, and staining, cells were detached one chamber at a time by a combination of shear force and protease cleavage. (A). Protease solution was driven into the inlet port (red circle) and detached cells from the chamber to be analyzed by flow cytometry (pink shade). The detached cells were then hydrodynamically focused by two sheath streams coming from the two sheath ports (yellow circles), before entering the point of detection for on-chip flow cytometry (red square). After all cells have been detached in the chamber shown in (A), the remaining chambers highlighted in (B-D) were detached and analyzed in that precise order as to avoid cross-contamination of samples between chambers.

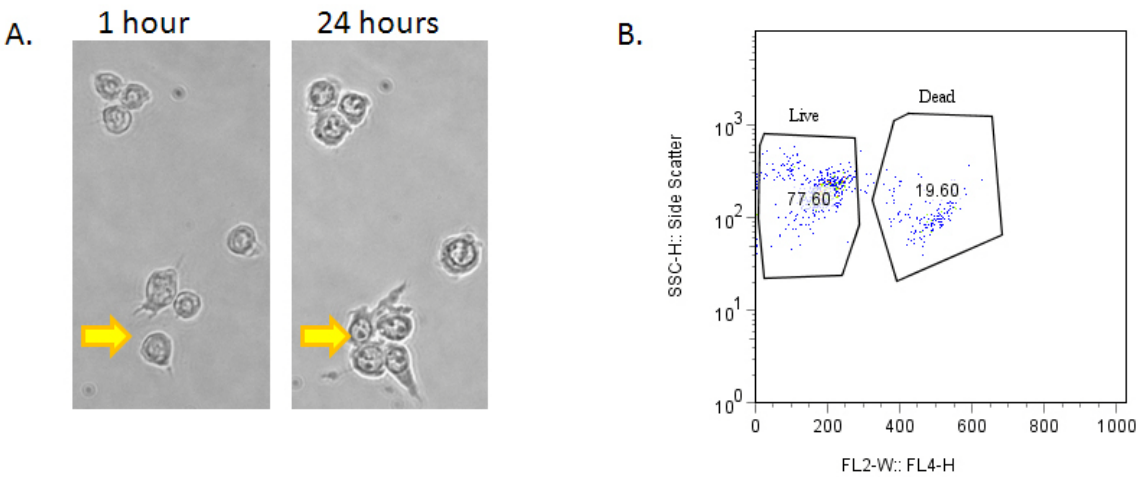

Figure 2.4. Cell viability after overnight culture on the platform. For overnight cell culture, the chip is coated with collagen, perfused with media saturated with 5% CO2, and is maintained in an air0tight configuration at a desired temperature (37 ±0.1 C) using thermal unit integrated in the chip manifold. In this experiment, macrophages (P388D.1 cell line) were cultured overnight on the microfluidic chip, and imaged the following morning prior to staining for dead cells (A). The yellow arrows indicate cell doublet after 24 h of on-chip culture, presumably resultant from cell division. The same cells were stained for dead cells and detached for flow cytometric analysis, and ~80% of the cells on the chip were viable (B).

Measurement of TLR4 pathway dynamics

The chip was validated by analyzing innate immune signaling elicited in macrophages (RAW264.7) upon challenge with Escherichia coli lipopolysaccharide (LPS), an agonist for the Toll-like receptor 4 (TLR4) pathway. TLR4 signaling forms the key innate immune response in defense against bacterial pathogens and its activation initiates with recognition of LPS by TLR4 followed by activation of kinases, nuclear translocation of transcription factors, and expression of proinflammatory cytokines.

TLR4 receptor activation kinetics*:* LPS binding causes TLR4-MD2 receptor to undergo a conformational change and oligomerization within seconds, as demonstrated in surface plasmon resonance experiments with purified proteins (*75, 76*). Reproducible measurement of such fast kinetics in a cell is nearly impossible to achieve using conventional detection methods, but our platform readily supported it. We used an innovative approach to monitor the kinetics using a monoclonal antibody which recognizes only the inactive form of the TLR4-MD2. Macrophages were challenged with LPS for 30 s, 1min, or 5min, and inactive TLR4-MD2 was stained with antibody for detection via on-chip flow cytometry (Fig. 2.5.A) and microscopy (Fig. 2.5.B). As expected, unstimulated macrophages showed highest antibody-mediated fluorescence. In contrast, macrophages exposed to LPS for as few as 30 s showed loss of antibody specific fluorescence (fluorescence histogram shifted to the left), and within 1 min, fluorescence levels decreased to background. These results indicate that, as *in vitro*, TLR4-MD2 receptors in intact cells are activated within

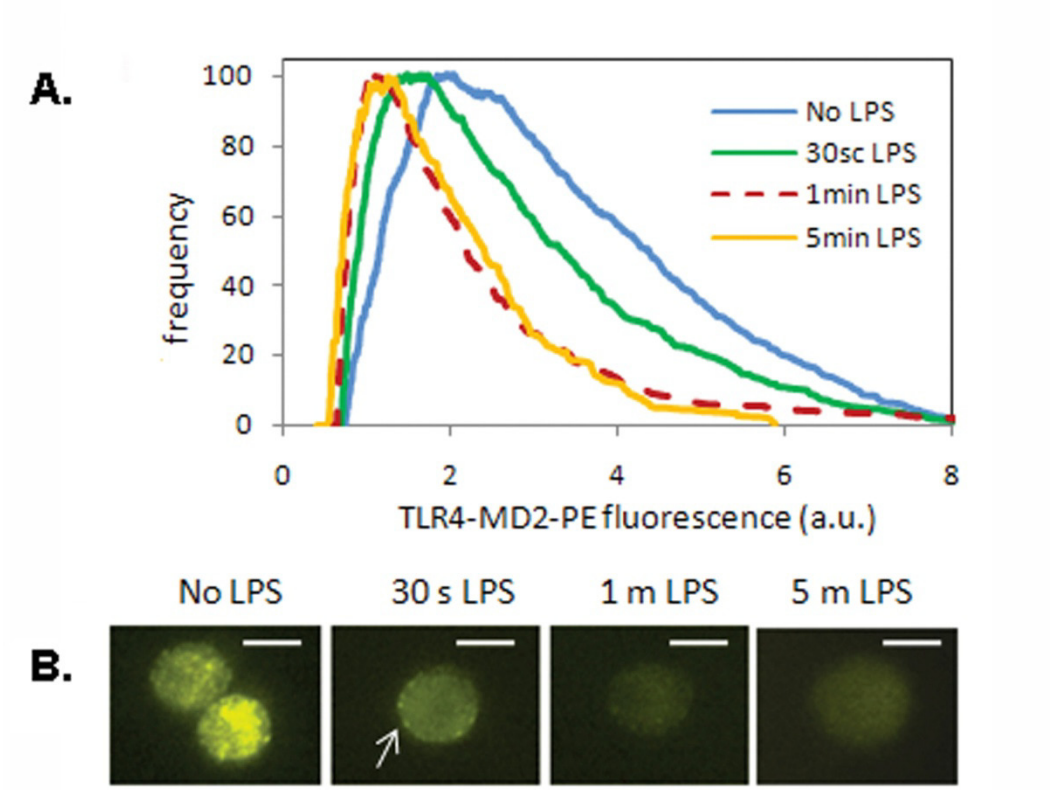

seconds of exposure to LPS. The on-chip flow cytometry collected quantitative measurements within minutes, and representative fluorescent images taken of the cells

Figure 2.5 LPS-stimulated activation of the TLR4-MD2 receptor complex was assessed at 30s, 1m, and 5m post-exposure, using on-chip flow cytometry (A). Note that in this assay activation of the TLR4-MD2 receptor leads to decreased levels of fluorescence, due to failure of the PE-labeled anti-TLR4-MD2 (MTS510) antibodies to recognize the activated receptor. Representative images of the cells used for flow cytometry were captured through immunofluorescence microscopy (B); PE staining decorates the macrophage surface (arrow) and decreases over time. Maximal reduction in PE fluorescence was observed at 1m post-exposure, with no further loss of fluorescence detected at 5m and beyond; this indicates that TLR4 receptor activation is complete by 1m. Scale bar = 10 μm.

prior to flow cytometry corroborates those measurements. Although the imaging analysis was qualitative in nature, they show localization of the TLR4/MD2 fluorescence to the cell membrane, which is information flow cytometry cannot provide, and further strengthens the validity of the TLR4/MD2 assay by showing the correct subcellular localization of the events measured.

Transient ERK phosphorylation kinetics: For profiling of ERK phosphorylation kinetics, which are considered intermediate events in the TLR4 pathway, we used on-chip phosphostaining assays adapted from the bench-scale version(*77*), and imaged the immunostained cells prior to the flow cytometry. Macrophages were exposed to LPS for 5 min, 30 min, 60 min, or to conditioned medium (negative control). Levels of ERK phosphorylation within individual cells were measured by staining with phospho-ERK antibody and measured using on-chip flow cytometry (Fig. 2.6.A). ERK phosphorylation was detected within 5 min of exposure to LPS, peaked by 30 min, and returned to near baseline level by 60 min. Qualitative representative immunofluorescence images (Fig. 2.6.B) of the same cells taken prior to on-chip flow cytometry agreed with the kinetics results shown in Fig. 3A, and showed abundance of phospho-ERK in the nucleus at 30 min, scale bar = 15 μm. Echoing the TLR4 receptor activation study, on-chip flow cytometry and imaging provided quantification and throughput with the added benefit of cellular localization information to yield greater sensitivity and dynamic range in measurement of ERK1/2 phosphorylation kinetics than using either method alone. On-chip results were further validated through conventional Western analysis (Fig. 2.6.C), showing increased ERK

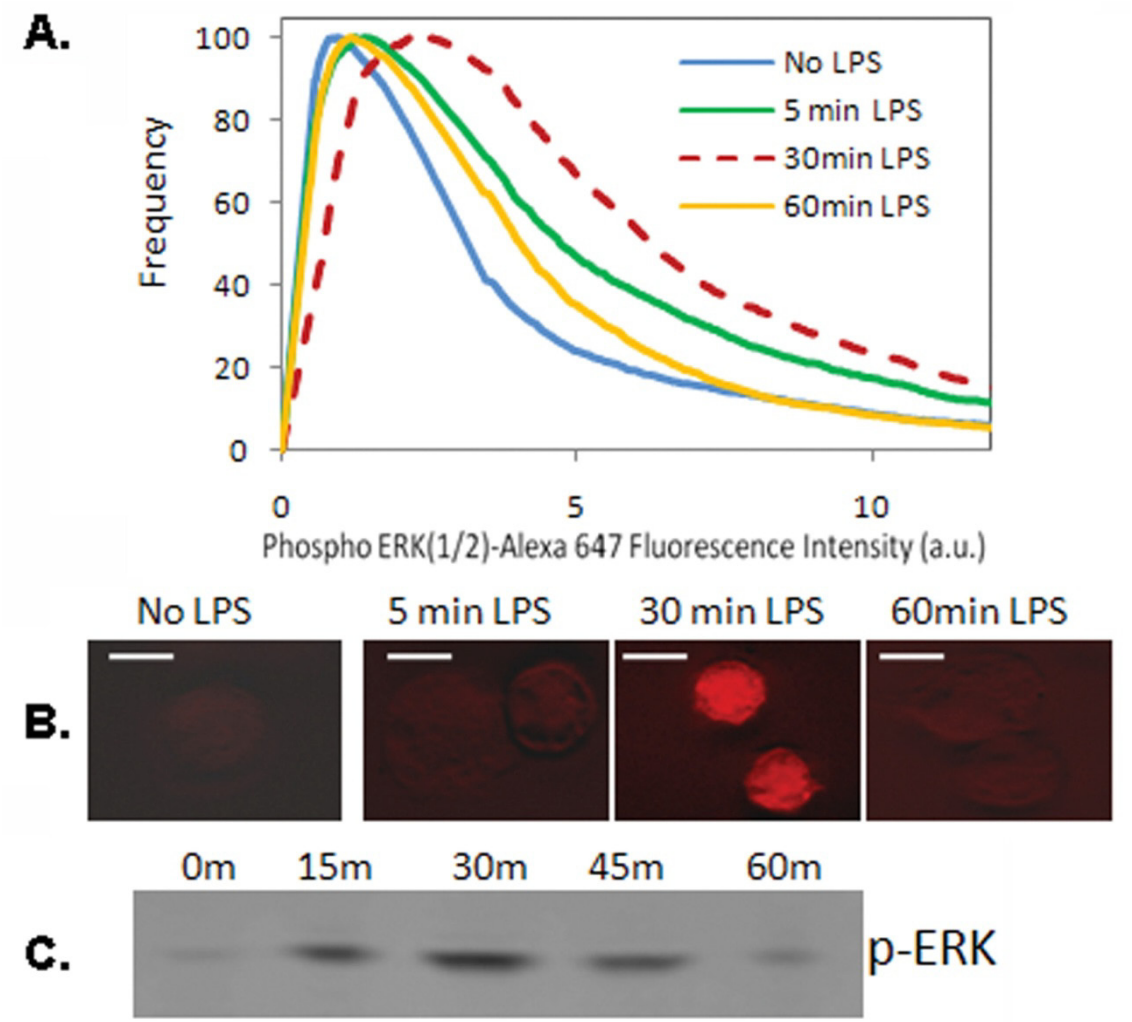

Figure 2.6 Flow cytometry analysis of ERK1/2 phosphorylation, detected using Alexa 647-labeled anti-phospho-ERK(1/2) antibodies. (A) Fluorescence was first detected by 5min post-exposure, peaked by 15m, and then returned to near-baseline levels by 60min. Immunofluorescence microscopy images (B) indicated that ERK phosphorylation was barely detectable by 5min, peaked by 30min, and returned to near-baseline levels by 60min. Scale bar = 15 μm. Both flow cytometry and imaging results were validated by traditional Western blotting (C).

phosphorylation that peaks at 30 min post LPS exposure, and the phosphorylation levels returned to basal levels by 60min. Flow cytometry and Western analysis using pan-ERK antibodies confirmed that ERK levels remained constant over the time-course of the experiment (not shown). The validation of chip-based results with traditional Western blot indicates that the chip platform can replace the labor-intensive Western blotting process and save not only time, but precious reagents to obtain single-cell resolution measurements of transient cell signaling events.

RelA-GFP translocation kinetics and intracellular cytokine measurement: RelA translocation is a transcription factor that translocates into the nucleus upon TLR4 activation and initiates transcription of proinflammatory genes including TNFα. The timing of RelA translocation was measured by monitoring the movement of green fluorescent protein (GFP) tagged RelA fusion protein stably expressed in macrophages. On our platform, we were able to multiplex real-time RelA-GFP translocation imaging with intracellular TNF-α measurement, and record both kinetic measurements from the same population of cells. During the first 2 hours of LPS incubation, time-lapse images of RelA-GFP were taken at 5 min intervals to provide more detailed translocation kinetics (Fig. 2.7), scale bar = 10 μm. The translocation of RelA-GFP can first be observed at approximately 15-20 min, and appears to peak starting at 45 min after initial introduction of LPS. Following the initial 2 hour LPS challenge, Brefeldin A was added to the LPS solution and TNF-α expression was measured using Cy5-labeled antibodies by flow cytometry (Fig. 2.8.A) and microscopy (Fig. 2.8.B), scale bar = 5 μm. The cells exhibited robust TNF-α

expression within 4 h of exposure to LPS. The timing of TNF-α expression was similar to that of TNF-α secretion by cells in absence of Brefeldin A, as determined through conventional ELISA (Fig. 2.8.C). The strong agreement between the chip results with the traditional ELISA measurements taken from cells grown in mammalian cell incubator (Fig. 2.8.C) indicates that the temperature and CO_2 controls on our platform is adequate for long term mammalian cell maintenance. The RelA translocation begins after TLR4 receptor activation, and coincides with the beginning of ERK1/2 phosphorylation at 15min, but RelA continues to translocate and remain in the nucleus long after the peak of intracellular ERK phosphorylation at 30 min. Since both RelA translocation and ERK phosphorylation are responsible for the induction of TNFα gene transcription, the increase in TNFα occurs later than both RelA translocation and ERK phosphorylation. The importance of incorporating real-time imaging into TLR4 pathway kinetics studies is that the timeline observed in a live cells from the same population can serves as a point of reference for other signaling events measured via end-point methods such as receptor activation and intracellular phosphorylation. The correlated kinetics measurements of many signaling events can then be used for the purpose of building a mathematical model the TLR4 pathway based on data collected from one cell population in a single experiment (Fig. 2.9).

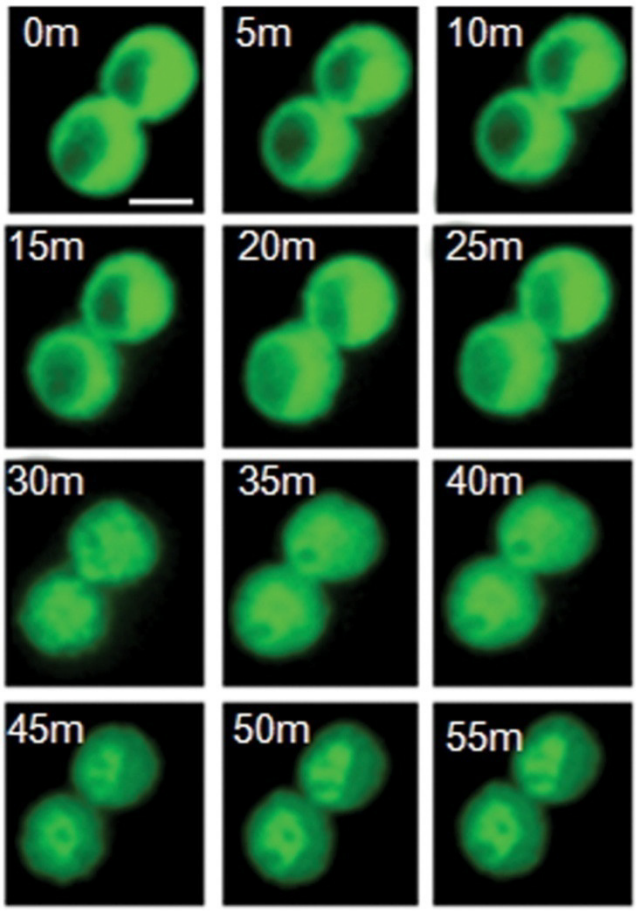

Figure 2.7 RelA-GFP nuclear translocation captured *via* time-lapse imaging. At 100 nM LPS, RelA-GFP translocation is observed starting at ~15-20min and saturating at ~45min. Scale bar = 10 μm.

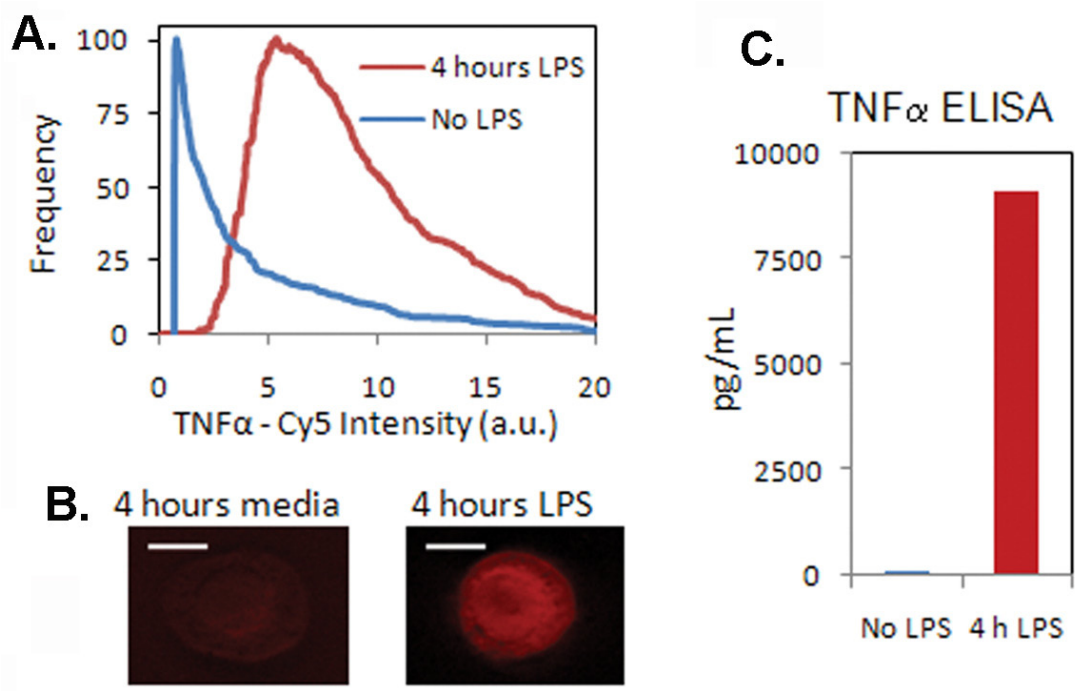

Figure 2.8. TNF-α expression at 4 h following challenge by LPS. Both cytometry (A) and microscopy analysis (B) yielded robust TNF-α-Cy5 signals at 4h post-exposure. Scale bar = 5 μm. (C) Conventional ELISA analysis of TNF-α expression by macrophages exposed to LPS for 4h validate the TNF-α expression measurements taken using the platform.

Simultaneous measurement of early, middle and late events in TLR4 pathway

Summarizing the results mentioned above, we found that LPS challenge of macrophages led to rapid activation of TLR4-MD2 (0.5-1 min), closely followed by activation of ERK (5-30min) and RelA (15-45 min), followed by return of ERK phosphorylation to baseline levels by 60 min, and then finally robust expression of TNFα at 4 hours. Having used the platform for analysis of the activation kinetics of individual steps within the TLR4 pathway, we then used it to capture, in a single experiment, a snapshot profile of the pathway's global dynamics (Fig. 2.9). The time-points (0, 30s, 30min, 4h) were chosen to represent both early and late events in the pathway (Fig. 2.9.A). Activation of pathway was assessed via live-cell imaging of RelA-GFP and via immunofluorescence microscopy (Fig. 2.9.E) and flow cytometry of TLR4-MD2 (Fig. 2.9.B), phospho-ERK (Fig. 2.9.C), and TNFα (Fig. 2.9.D). Consistent with our previous results, we observed TLR4-MD2 activation at 30s, ERK and RelA activation at 30min, and TNFα expression at 4h.

Mathematical Modeling

To investigate the flow of information through the TLR4 signaling pathway and to predict the timing of events, we treated the TLR4 pathway as a Boolean network, with nodes profiled in this study shown in red (Fig.2.10.A). The results from our Boolean model of the TLR4 network agree with our experimental results. The model clearly predicts order of signaling events we experimentally observe with activation being the earliest timed-event, followed by transient MAP kinase activation, leading to TNF-α production (Fig.2.10.B), showing that our microfluidic platform can replace cumbersome, expensive macro-scale assays to profile many nodes of a given

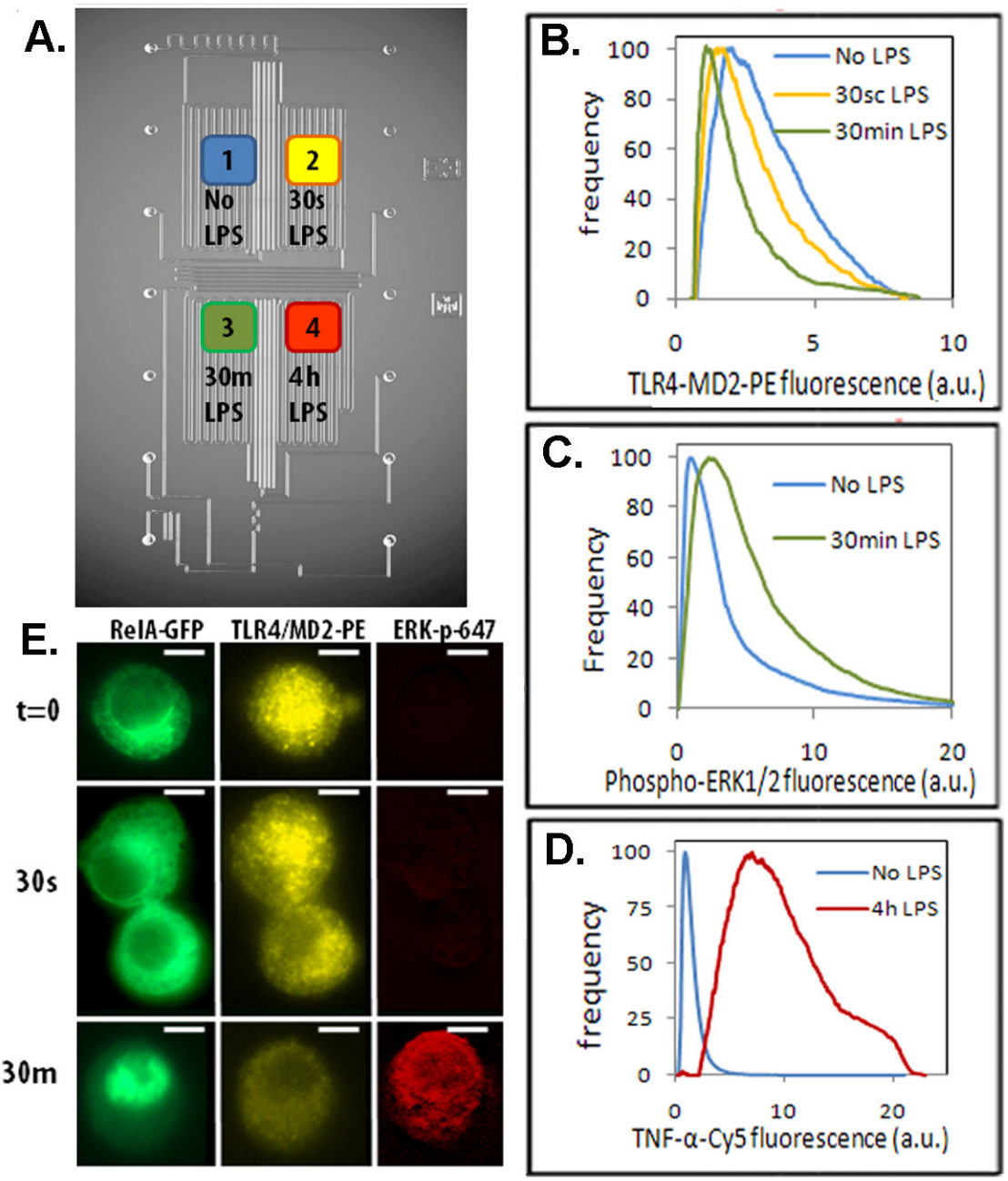

Figure 2.9. A. Snapshot of the entire TLR4 pathway taken in one chip experiment using time points 0, 30s, 30min, and 4h. Flow cytometry overlays for TLR4 activation(B), ERK phosphorylation(C), and TNFα production(D). Representative images of macrophages showing translocation of RelA-GFP, loss of inactive TLR4/MD2-PE, and increase of ERKp-647 are shown in E.

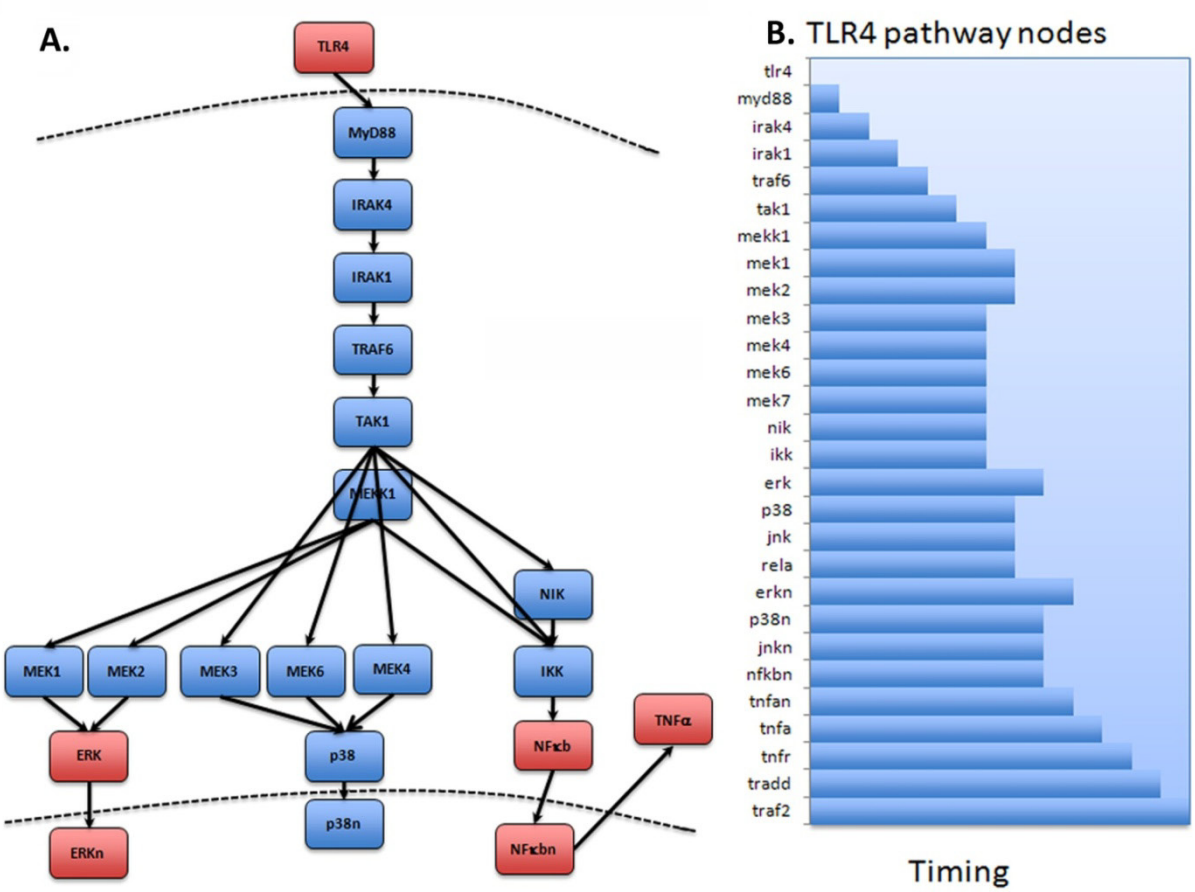

Figure 2.10. A. Simplified TLR4 network treated as a Boolean network. Each node (protein) in the pathway was allowed multiple inputs and multiple outputs, and all nodes were represented as OR gates in which any single input to the node stimulated all output from the node. The network was simulated in Matlab® using the Matlab RBN Toolbox. B. Simulation results predict the timing of activation of each node in the network. Nodes profiled in this study are highlighted in red.

signaling pathway in one experiment, producing temporally correlated data usable for mathematical modeling.

2.5. Conclusions

Our platform was validated by profiling TLR4 pathway from receptor activation to cytokine production; however, its ability to perform multiple biochemical measurements of phosphorylation, translocation and cytokine production in a single cell population makes it widely applicable to interrogating other pathways and cellular functions at a systems level. The two orthogonal methods of detection - on-chip flow cytometry and live cell fluorescence imaging work synergistically to combine the quantitation and throughput of flow cytometry with real-time cell signaling kinetics that can be used to correlate all other end-point measurements in the same experiment. The platform was benchmarked against gold-standard conventional assays and the on-chip results were in excellent agreement with those obtained by western assays and ELISAs. Many time- and labor-intensive biochemical steps (such as centrifugation) have been replaced with a versatile, reusable chip that integrates and automates cell culture, preparation and analysis. The real-time imaging capability provides a means to track health of cells and also provide complimentary data to confirm cytometry results. Furthermore, the ability to perform assays with minimal numbers of cells (<5000) makes it an ideal solution for analysis of primary cells and rare cell types, and highly efficient use of costly antibodies (100x lower amounts needed than Western or ELISA) is particularly advantageous when carrying out large numbers of experiments. Finally, the platform is completely self-contained and has a small footprint, making it ideal for experiments with highly pathogenic organisms in bio-containment laboratories (BSL3 or 4).

Chapter 3.

Microfluidic assay for the detection of metabolically labeled O-linked N-acetylglucosamine modified proteins

3.1. Abstract

The modification of serine and threonine residues in nculeocytoplasmic proteins with a single GlcNAc residue is an important post-translational modification with functional consequences. We present a novel microfluidic method that can detect specific O-GlcNAc modified proteins without custom site-specific O-GlcNAc probes such as monoclonal antibodies. We demonstrate the metabolic labeling of nuclear pore protein nup62 with azide-modified glucosamine (O-GlcNAz), followed by copper based click chemistry labeling of the azide sugar with biotin. The detection of the O-GlcNaz modified nup62 is achieved by using proximity ligation assay (PLA), employing one antibody probe directed against nup62 and one streptavidin probe directed against the O-GlcNAz-biotin, to achieve dual recognition. The resultant PLA signal is then quantified using on-chip flow cytometry. The strategy developed in this chapter for detecting specific O-GlcNAcylated proteins in intact cells will prove useful for identifying and elucidating O-GlcNAcylated proteins, and shed light on their importance in cell signaling regulation.

3.2. Introduction

The modification of proteins with an O-linked N-acetylglucosamine (O-GlcNAc) monosaccharide is a unique type of post-translational modification that occurs in intracellular proteins. The O-GlcNAc modification was first described by Gerald Hart and colleagues in 1984(*78*). Since then a number of studies have focused on identifying O-GlcNAcylated proteins and understanding the role of O-GlcNAcylation in cellular and disease processes(*79*). O-GlcNAcylation has the following unique features: (1) In eukaryotes, O-GlcNAc modification is primarily found in nuclear and cytoplasmic proteins. (2) Unlike complex N-linked or O-linked glycosylation, O-GlcNAc does not extend into larger, more complex multi-multioligosaccharide structures. (3) O-GlcNAcylation is a highly dynamic modification that occurs on Ser/Thr residues of proteins, analogous to phosphorylation of proteins. The majority of O-GlcNAcylated proteins are modified in response to cell signaling cues, such as growth factors, signaling molecules, nutrient fluxes, and stress. O-GlcNAcylation therefore has significant effects in cell signaling, metabolism, transcriptional regulation, cell cycle control, and cellular structure(*80*). Like phosphorylation, O-GlcNAc modification of proteins has been shown to play key roles in regulating protein activity. (4) There is an increasing body of evidence that indicates a dynamic interplay between O-GlcNAcylation and phosphorylation and this crosstalk between the two post-translational modifications has been shown to have a functional significance in the signaling of the protein(*81*). (5) Finally, similar to phosphorylation that is regulated by protein kinase/phosphatase activities, O-GlcNAcylation is also controlled by the activities of two specific

proteins. The addition of the O-GlcNAc is catalyzed by a glycosyltransferase named O-linked N-acetylglucosaminyltransferase (OGT), and the removal catalyzed by the antagonistic β-N-actylglucosaminidase (O-GlcNAcase) (figure 3.1) (*82-84*). OGT is a highly conserved protein among different species and uses UDP-GlcNAc as the donor sugar to transfer GlcNAc onto the Ser/Thr residues of substrate peptides/proteins.

Significance in lymphocyte activation

A number of studies have demonstrated a functional role for O-GlcNAcylation in chronic diseases such as cancer, diabetes and neurodegenerative disorders(*79*). More recently, reports have demonstrated an increasing role for O-GlcNAc modification of proteins in the regulation of both innate and adaptive immune signaling(*85*). Activation of neutrophils has been shown to increase levels of O-GlcNAcylation that in turn correlate with increased neutrophil motility(*86*). As early as 1991, studies demonstrated that activation of T-lymphocytes caused a rapid increase in levels of nuclear and cytoplasmic O-GlcNAcylation(*87*). More recent studies have identified specific signaling proteins, such as NFAT and NFkB, which are O-GlcNAcylated in response to T-cell receptor (TCR) dependant activation of T-lyphocytes and B-cell receptor (BCR) dependant activation of B lymphocytes(*88*).

In lymphocytes, mitogen or antigen activation rapidly decreased O-GlcNAcylation of cytoplasmic proteins, while concurrently increasing O-GlcNAcylation of many nuclear proteins(*87*). RNAi knock-down of OGT in T cells lead to impaired NFAT and NFkB activation, resulting in a reduction of IL-2 production and impaired T-cell

activation(*88*). Knock-down of OGT also prevented early B cell activation, whereas overexpression of OGT lead to enhanced B cell receptor-dependent activation of NFkB. It is postulated that the O-GlcNAcylation of NFAT and NFkB is required for their translocation into the nucleus, but whether the O-GlcNAc modification is competing with phosphorylation or working in concert with phosphorylation to trigger translocation of NFAT and NFkB is still unknown.

Methods for detecting and profiling O-GlcNAc modified proteins

The reason for the slow progress in the field of O-GlcNAc modification in cell signaling is due mostly to a lack of efficient methods for detection of O-GlcNAcylated proteins. Unlike charged PTMs such as phosphorylation, O-GlcNAc addition or removal does not significantly alter the migration pattern of proteins on SDS-PAGE gels. Also, the ubiquitous cellular hydrolases efficiently remove O-GlcNAc from proteins when the cell is damaged or lysed. Therefore, O-GlcNAc modifications are often lost during the process of protein purification prior to bioanalytical studies. The most popular methods currently in use for detecting O-GlcNAcylated proteins are mass spectrometry based O-GlcNAcomics, and immunoprecipitation (IP) using monoclonal antibody directed against O-GlcNAcylated Ser/Thr residue(*89*). Mass spectrometry based methods are highly sensitive, and are extremely useful for detection and site mapping of O-GlcNAcylated proteins. However, these approaches are expensive to run and require specialized equipment and expertise. A novel method that allows detection of O-GlcNAcylated

proteins within an intact cell will overcome these obstacles and provide immense value to the field.

Metabolic labeling of proteins using bioorthogonal probes

Metabolic labeling of O-GlcNAc-modified proteins using bioorthogonal probes was pioneered by the Bertozzi group(*90*). Tetraacetylated synthetic sugars whose N-acyl side chain is modified with an azide moiety can be taken up by cells in culture, and processed into azido sugar containing substrates whose sugar residues are incorporated into cytoplasmic and nuclear proteins (figure 3.2.A). The azide group on the glucosamine is a bioorthogonal chemical handle that can be conjugated to detection molecules for downstream biochemical analysis. A number of different chemistries are now available for coupling to the azide moiety on O-GlcNAcylated proteins. These include Staudinger ligation which uses phosphine for crosslinking the azide, copper catalyzed 1,3 dipolar azide-alkyne cycloaddtion and copper-free cycloaddition reaction. Among these, the copper based cycloaddition reaction remains the most popular click chemistry reaction, particularly for experiments that do not require live cell labeling. By using alkyne molecules conjugated with fluorescent dyes or biotin, the azide labeled proteins can be easily detected *via* copper based click chemistry.

Detection of changes in O-GlcNAc levels in specific proteins

Detection of all O-GlcNAcylated proteins in the cell can be done using the metabolic labeling approach described above, or via the use of the monoclonal antibody directed against synthetic peptide containing serine-O-GlcNAc. Detection

of specific O-GlcNAc modified proteins however, is made complicated by the lack of reagents. Unlike phosphoproteins, O-GlcNAcylated proteins do not have a readily available repertoire of commercially available site specific O-GlcNAc antibodies, hence the simple question "is my protein O-GlcNAc modified?" can only be answered by immunoprecipitating with O-GlcNAc antibody followed by probing with antibody directed against the protein of choice. As mentioned earlier, such immunoprecipitation experiments are labor intensive, and require homogenized cell lysates. To overcome these limitations, in this study,we have developed proximity ligation assay (PLA) to detect specifically O-GlcNAc modified proteins in intact cells. The PLA method has been used for visualizing phosphorylations(*91*) with high selectivity without the use of site-specific phospho-antibody. The basis for PLA is the use of proximity probes made of antibodies attached to oligonucleotides — one directed against the protein and the other directed against the PTM, to target post-translationally modified proteins by dual recognition. When both probes bind a protein with PTM, the two oligonucleotides can then be ligated to two additional linear nucleotides to form a circle. For detection, one of the antibody-attached oligonucleotides serve as a primer for phi29 DNA polymerase, which generates a long single-stranded concatemers by rolling circle amplification (RCA). The concatemers can then be detected by hybridizing fluorephores labeled oligonucleotides, and analyzed via microscopy and flow cytometry. The adaptation for *in situ* PLA for detection of O-GlcNAcylation allows glycobiologists to circumnavigate the use of custom O-GlcNAc-specific antibodies.

Microfluidic PLA assay for detection of specific O-GlcNAcylated proteins The microfluidic PLA assay described in this chapter combines metabolic labeling of cells with bio-orthogonal reporters such as GlcNAz. Coupled with flow cytometry and imaging, our assay not only quantifies changes in levels of O-GlcNAc in specific proteins but can also be used to study the localization of the O-GlcNAcylated proteins. The following is a brief description of the assay developed to detect and quantify O-GlcNAc on a single protein of interest. After metabolic incorporation of O-GlcNAz in cells (Figure 3.2.A), the azide handle on O-GlcNAcylated proteins is reacted with alkyne molecules conjugated to biotin via copper catalyzed click chemistry to form a stable triazol biotin conjugated O-GlcNAz modified protein. (figure 3.2.B). Then, a custom PLA probe is generated by conjugating streptavidin to the MINUS oligonucleotide. The PLA assay proceeds with the binding of monoclonal antibody directed against the protein, followed by addition of the other PLA probe to the antibody and the custom streptavidin PLA probe to the biotin on the azide. The two PLA probes are then ligated, and the circular template is amplified by rolling circle amplification, generating fluorescent concatemers detectable by flow cytometry (figure 3.2.C).

Bioorthogonal labeling of T lymphocyte nuclear proteins and detection via proximity ligation assay

In this study, we have used Jurkat cells as a model T-lymphocyte cell line since these cells are known to express O-GlcNAcylated proteins in detectable levels even in unstimulated cells. In order to validate our PLA assay, we set up a proof-of-principle

experiment to detect the O-GlcNAc levels in nuclear pore glycoproteins (Nup62 in particular). This model system was chosen for two reasons: (1) Nup62 is one of the most heavily O-GlcNAcylated proteins. In fact, it is believed that this nucleoporin has as many as 10 O-GlcNAc sites. (2) Bertozzi and colleagues have previously reported that the OGT enzyme is able to utilize UDP-GlcNAz to transfer GlcNAz onto Ser/Thr residues in Nup62. They further demonstrated that in Jurkat cells which were metabolically fed with tetraacetylated GlcNAz, the GlcNAz was incorporated into the Nup62 glycoprotein as detected by Staudinger ligation using labeled phosphine.

In addition, we study the effect of an inhibitor of O-GlcNAcase (OGA) on the levels of O-GlcNAcylation in Nup62. As mentioned previously, OGA is the enzyme that catalyzes the removal of O-GlcNAc from peptides/proteins. Therefore, an inhibitor of OGA would increase the stoichiometry of O-GlcNAcylation in intracellular proteins. Indeed, OGA inhibitors have been shown to increase global levels of intracellular O-GlcNAcylation in a number of different cell types. A number of small molecule OGA inhibitors have been synthesized with varying degrees of specificity towards OGA. One inhibitor, O-(2-acetamido-2-deoxy-Dglycopyranosylidene) amino-N-phenylcarbamate or PUGNAc has been the OGA inhibitor of choice for a number of *in vitro* studies. However, PUGNAc suffers from a low selectivity towards OGA. A recent study synthesized a more potent, extremely stable and highly specific OGA inhibitor, Thiamet G, which is also soluble in aqueous buffers. Using *in vitro* and in vivo experiments, the researchers demonstrated the potency of the drug in inhibiting OGA(*92*). In our study, we will pre-treat the cells

with thiamet G and will use our PLA assay to examine if the inhibitor causes an increase in O-GlcNAcylation levels in Nup62.

3.3. Materials and Methods

Metabolic labeling of Jurkat cells

Jurkat cells were purchased from ATCC (TIB-152), and cultured in RPMI media (11875-093, Invitrogen) containing 10% FBS (100-500, Gemini) and 0.5 mg/ml penicillin and streptomycin (15240062, Invitrogen). Cells were kept in a humidified incubator maintained at 5% CO_2. For bioorthogonal labeling, Jurkat cells were seeded at $2.5x10^4$/mL in growth media containing tetraacetylated N-Azidoacetylglucosamine or GlcNAz (88903, Pierce) for 72 hours. For negative control, Jurkat cells were grown in media containing DMSO vehicle for 72 hours. Bioorthogonally labeled cells and control cells were then pelleted at 300g, and washed twice in PBS prior to loading into microfluidic chip.

Microfluidic chip design and platform setup

The six chamber microfluidic chip (figure 1.4.C) was designed in-house using AutoCAD 2010 (Autodesk Inc., San Rafael, CA), photomasks were generated at Photo Sciences (Torrence, CA), and quartz microfluidic devices were fabricated by Caliper Life Sciences (Hopkinton, MA). An array of fourteen holes 500 μm in diameter, seven on each side, provided for fluid inlet. All subsequent steps in chip packaging and details of the chip platform are as previously described (*17, 93*).

Microchip surface treatment with Cell-Tak™

The 6 chamber microchip was cleaned with 10% bleach in filtered DI water for 15 min, followed by flushing with DI to wash off all residual bleach. To make the Cell-Tak™ (354240, BD Biosciences) solution, combine 15µl Cell-Tak™ with 575µl 0.1M sodium bicarbonate pH 8.0, followed by adding 10µl of 1N NaOH immediately prior to adsorption onto chip. Flow Cell-Tak™ solution into chip for at least 15min, followed by PBS flush for 5 min. Bioorthogonally labeled Jurkat cells are flown into the chip and captured to the cell surface for subsequent Click-IT labeling and proximity ligation assay.

Copper Click-it labeling of GlcNAz with biotin

After loading into the chip, Jurkat cells were fixed with 4% paraformaldehyde in PBS, then permeabilized with 0.25% Triton-X 100 (X100-100ML, Sigma) in PBS for 10 min. After permeabilization, cells were blocked with 2% BSA in PBS, and then 30 min incubation of freshly made Click-iT reagent made according to manufacturer's instructions (C33367, Life Technologies). After Click-iT labeling of GlcNAz with biotin, the cells were washed with 2% BSA solution for 5 min.

Proximity ligation assay for detection of azidoglycosylated proteins

Streptavidin PLA probes were generated by conjugating the MINUS PLA probe maker (92010-0020, Olink). Nup62 antibody (ab56982, abcam) antibody was diluted to 10µg/mL in 2% BSA in PBS, and flown into the predetermined chambers and incubated for 1 hour at 37°C. After the 1 hour incubation, the chip was washed with TBS with 0.025% Tween for 5 min. The following PLA solution was made fresh: 2 µL of 42ug/mL Strept-MINUS probe, 10 µL mouse-PLUS probe, 38 µL dilution buffer from PLA kit. Load PLA solution into chambers for detection of dynamically

glycosylated Nup62. Incubate cells with PLA solutions for 1 hour at 37°C, followed by 5min wash with TBST. The ligation and amplification steps are performed according to manufacturer's instructions, using 1 reaction for all 6 chambers.

Microscopy and image analysis

Prior to imaging, the cells were incubated with Hoechst stain (33342, Pierce) in PBS for 10min, followed by 10 min wash in PBS. Epi-fluorescent images were captured at 60X magnification on an Olympus IX-71 microscope equipped with GFP and DAPI filters and Hamamatsu ORCA-R2 cooled CCD camera. Images were artificially colored and overlaid in ImageJ.

Flow cytometry

After microfluidic chip based sample preparation, the cells were detached using a combination of shear force and proteolytic cleavage with 100 μg/mL elastase (I.U.B.: 3.4.21.36,Worthington). The cells were then analyzed using BD FACscan and the data was analyzed using Flowjo.

3.4. Results and discussion

Metabolic labeling of proteins with tetraacylated azidoglucosamine (Ac_4GlcNAz). Jurkat cells were maintained in media containing 40 μM Ac_4GlcNAz for 72 hours. The tetra-azido glucosamine diffuses across the cell membrane and is converted to azidoglucosamine by the nonspecific esterases in the cytoplasm, and the azidoglucosamine is added to proteins by the cell's own glycosylation machinery. The azide group on the incorporated GlcNAz is a bioorthogonal handle that is later used for detection. during which incorporation of GlcNAz into intracellular proteins takes place inside the cells. To detect the GlcNAz, cells were fixed and permeabilized, and alkyne-alexa488 was used to label the metabolically incorporated GlcNAz. Three concentrations of alkyne-alexa488 were used for the click chemistry labeling of GlcNAz as shown in figure 3.3. 2.5 μM of alkyne-alexa488 showed the biggest increase in fluorescence attributed to GlcNAz labeling. For subsequent GlcNAz-Nup62 PLA assays, 2.5 μM alkyne-biotin was used as the probe to label the GlcNAz on Nup62 with biotin.

Anti-Nup62 antibody concentration optimization

To optimize the concentration of Nup62 antibody to use for the PLA assay, 10, 20, 40 μg/mL Nup62 antibody concentrations were compared to the equivalent IgG control in a single antibody PLA assay, where both PLA plus and minus probes are directed against the same species (figure 3.4). Since all Nup62 concentrations showed similar shifts from IgG controls, the lowest concentration of 10 μg/mL was chosen for subsequent Nup62/azidosugar PLA experiment.

PLA detection of O-GlcNAz modified Nup62

Jurkat cells were fed with media containing 40μM Ac_4GlcNAz or DMSO vehicle for 72 hours. Following feeding with azide sugar, the Jukat cells were fixed, and h=loaded into the microfluidic chip pre-coated with Cell-Tak™. The O-GlcNAz modifications on Nup62 proteins were labeled with alkyne-biotin using copper based click chemistry using the same experimental conditions optimized use alkyne-alexa488. After the biotin labeling of GlcNAz, 10 μg/ml of Nup62 antibody is incubated with the cells to achieve dual recognition of O-GlcNAz modified Nup62. For the PLA detection, a streptavidin PLA probe and an anti-mouse PLA probe were used to bind the biotin -GlcNAz and monoclonal antibody bound to Nup62 protein. The two probes are ligated to form a circle and generate fluorescent concatemers via rolling circle amplification (figure 3.2.C). Streptavidin without oligonucleotide and IgG antibody were used as controls for PLA. Figure 3.5 shows that both IgG (orange histogram) and streptavidin (green histogram) controls yielded equivalent background fluorescence, but the metabolically labeled Nup62 showed the highest PLA fluorescence (blue histogram). As expected, the cells fed with DMSO vehicle instead of Azide sugar showed the lowest level of fluorescence (red histogram).

Thiamet G mediated increase of Nup62 O-GlcNAz incorporation

To show that the PLA assay can be used to detect changes on specific proteins with O-GlcNAz modifications, metabolically labeled Jurkat cells were treated for 24 hours with 50 μM of OGA inhibitor Thiamet G (figure 3.6). Thiamet G treated cells (red histogram) displayed more PLA mediated fluorescence than metabolically labeled cells without Thiamet G treatment. The flow cytometric results are corroborated with fluorescence microscopy. Figure 3.7 shows extensive duorecognition of O-GlcNAz

modified Nup62 with PLA assay in Ac_4GlcNAz fed cells (figure 3.7.B), and loss of O-GlcNAz-Nup62 signal in Thiamet G treated cells (figure 3.7.C).

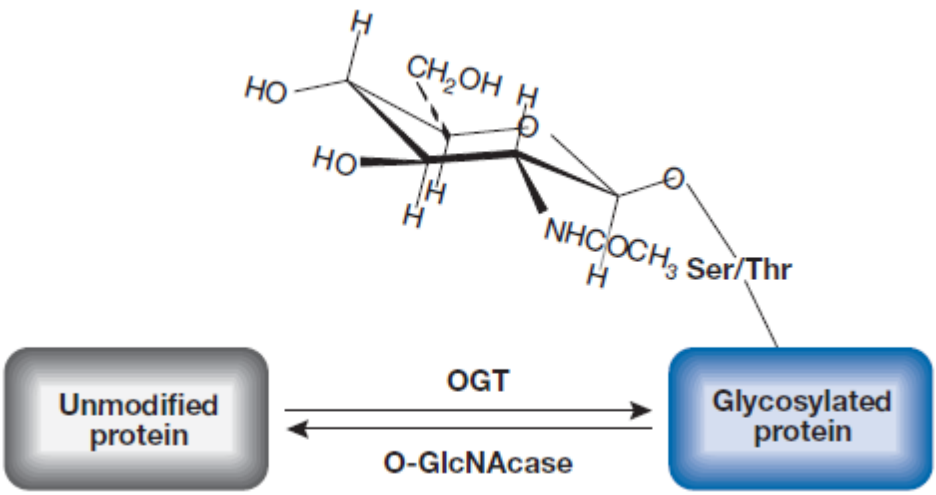

Figure 3.1 The addition of O-GlcNAc to proteins is catalyzed by OGT, and the removal of O-GlcNAc is catalyzed by OGA. The O-GlcNAc modification process is dynamic and can influence protein function(*85*).

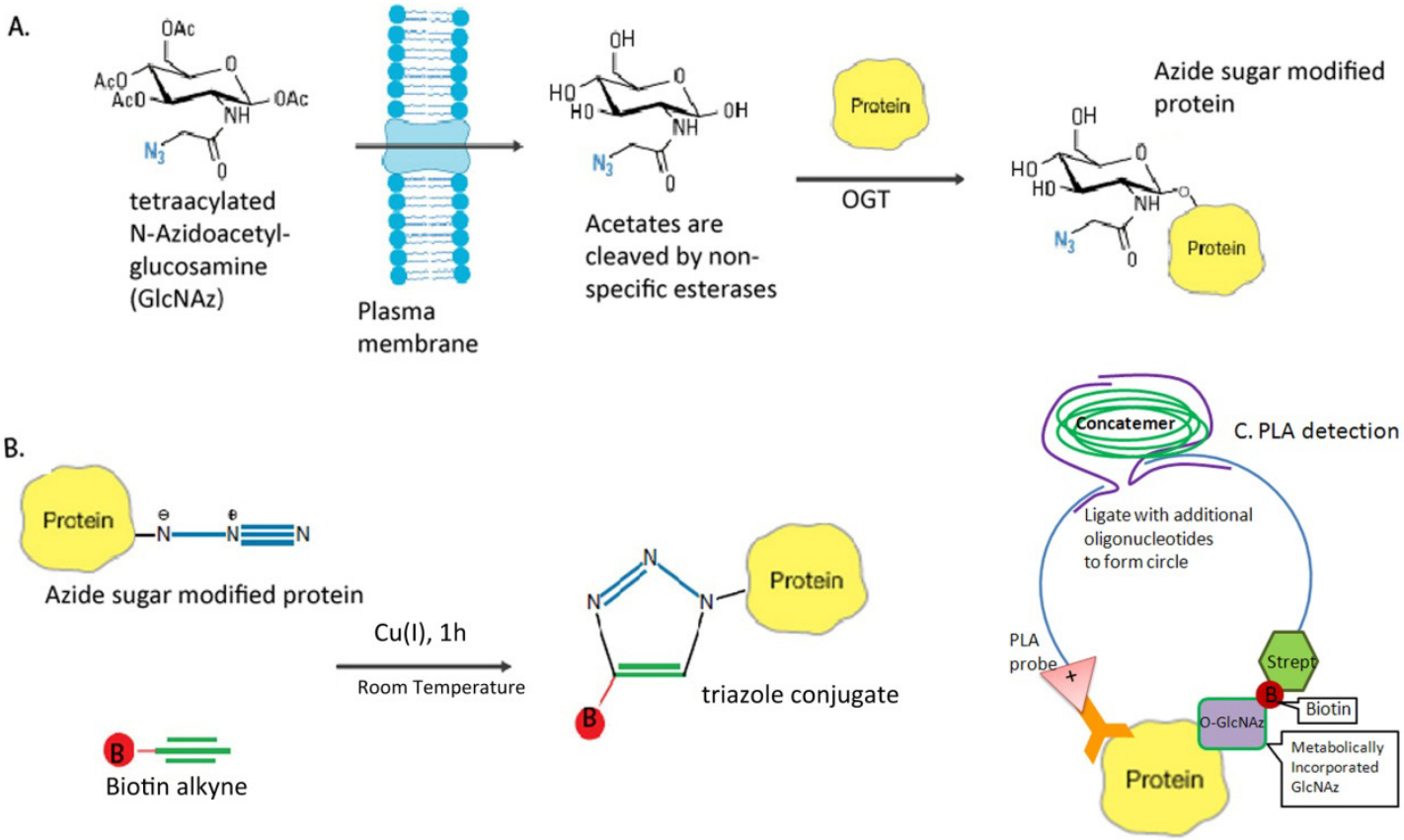

Figure 3.2 Schematic diagrams of chemical reactions used for assay development to detect specific dynamically O-glycosylated proteins. A.The metabolic labeling of proteins with GlcNAz. Tetra-azido glucosamine is added to the cell culture media, and is taken up by the cells. Nonspecific esterases in the cytoplasm cleave off the acetyl goups, leaving azidoglucosamine that is added to proteins by the cell's own glycosylation machinery. The azide group on the incorporated GlcNAz is a bioorthogonal handle that is later used for detection. B. Copper click chemistry of the addition of biotin-alkyne to the azide group on the protein-bound azidoglucosamine. C. Detection of specific GlcNAz-biotin labeled proteins using proximity ligation assay. The concatemers generated from the circular DNA template can be detected with fluorescent hybridization probes.

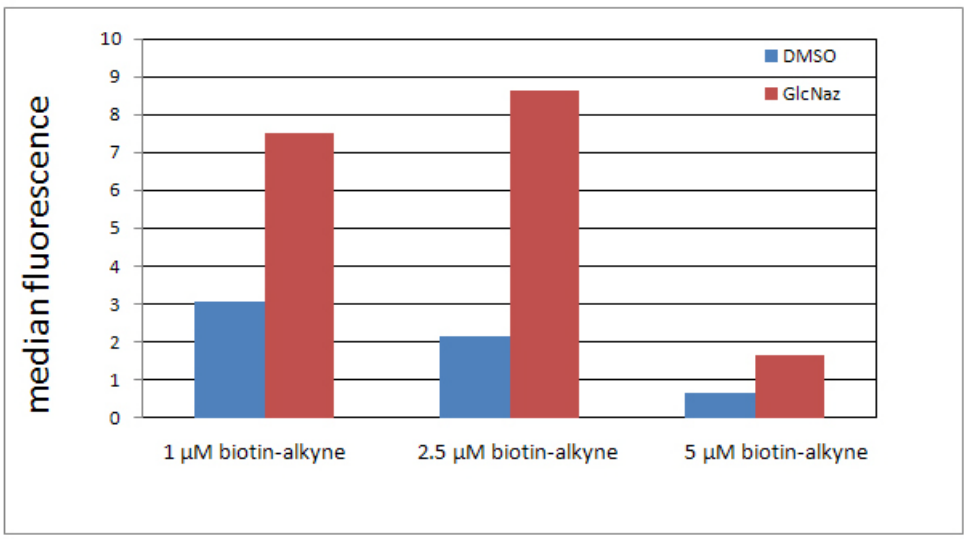

Figure 3.3 Optimization of the metabolic labeling of Jurkat cells with GlcNAz, and detection by conjugation to biotin-alkyne using Click-it chemistry. Once the biotin is covalently conjugated to the GlcNAz, streptavidin-488 was added to generate a fluorescent signal. At 2.5 µM biotin-alkyne concentration, cells treated with GlcNAz showed the largest shift from background.

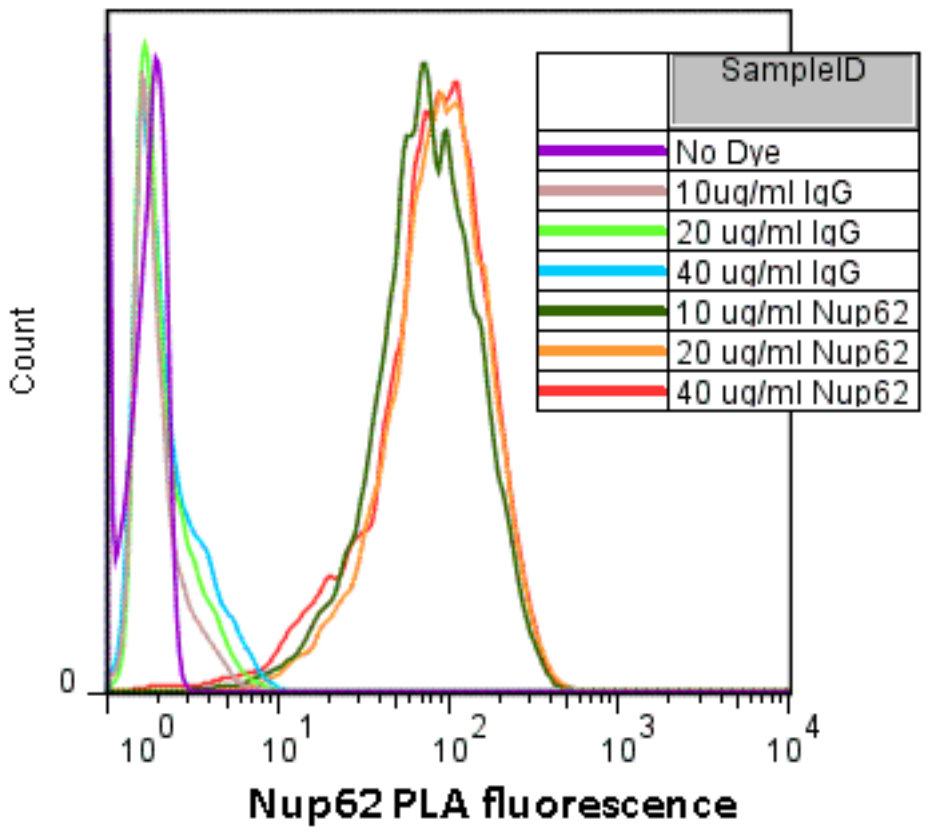

Figure 3.4 Optimization of anti-Nup62 antibody concentration for proximity ligation assay. The lowest Nup62 antibody concentration is sufficient to produce PLA signal.

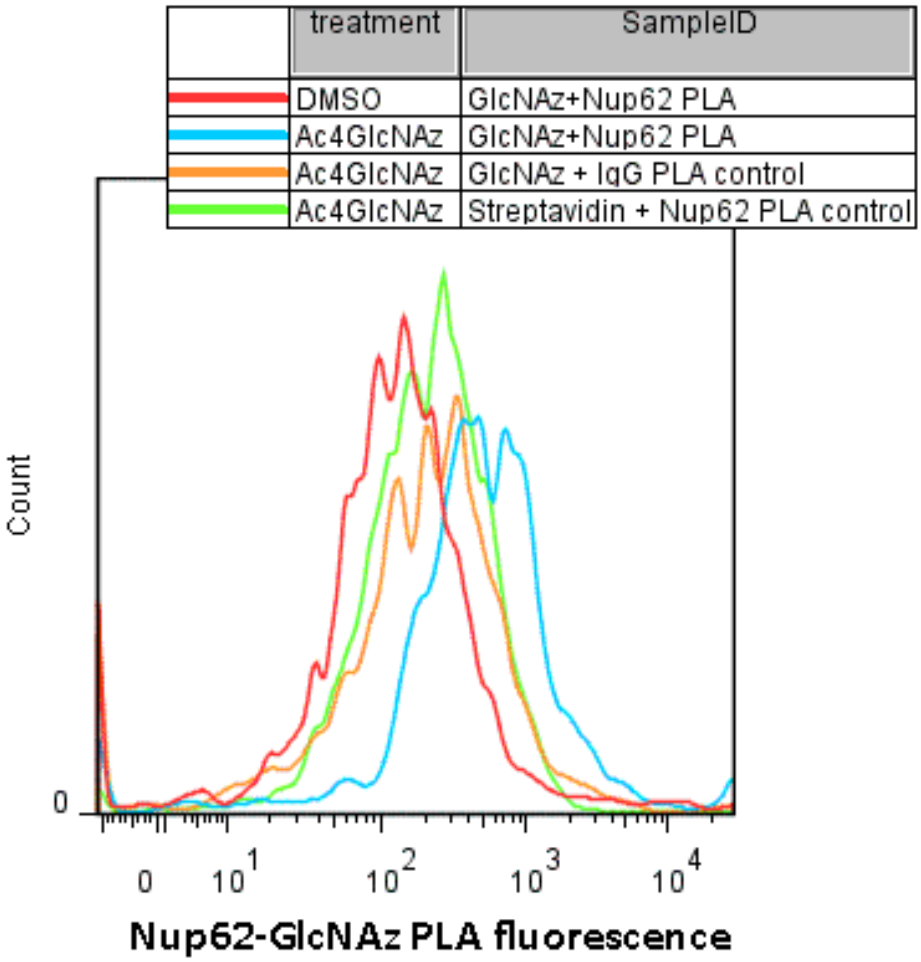

Figure 3.5 Microfluidic flow cytometry based detection of GlcNAz modified Nup62 using proximity ligation assay. The Azide sugar labeled Nup62 showed the largest PLA signal (blue histogram, shifted furthest to the right) compared to controls.

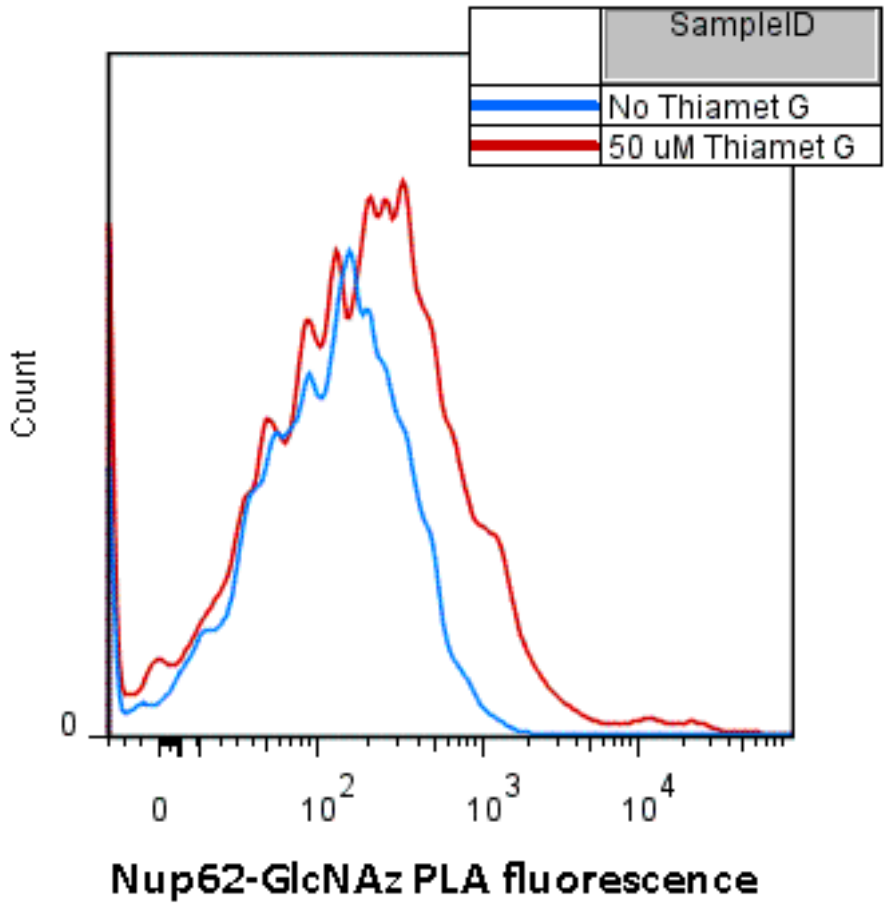

Figure 3.6 PLA assay of cells fed with 40 μM Ac_4GlcNAz for 72 hours and treated with 50 μM OGA inhibitor Thiamet G for the last 24 hours. The Nup62-GlcNAz PLA signal in cells treated with Thiamet G show increase in O-GlcNAz levels due to inhibition of its removal by OGA.

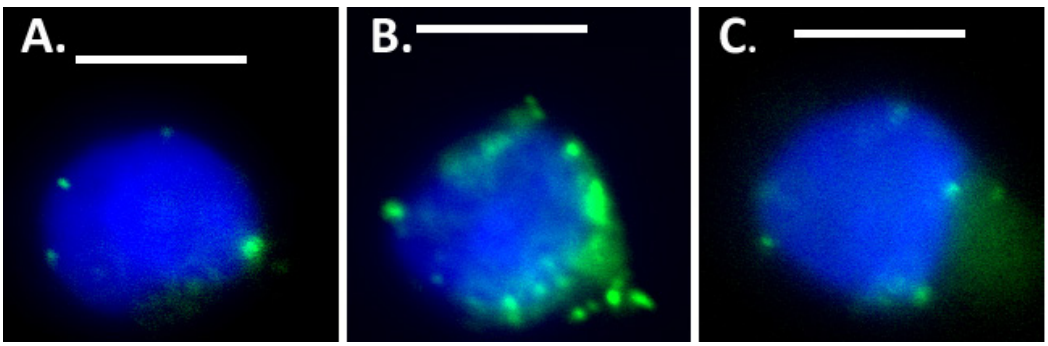

Figure 3.7. Fluorescence images of cells with metabolically labeled O-GlcNAcylated Nup62. Green – O-GlcNAz-Nup62 PLA signal, blue – nucleus. All scale bars = 10 μm. A. When cells are fed only DMSO for 72 hours, there is minimal GlcNAz/Nup62 PLA signal. B. Cells fed with 40 μM Ac_4GlcNAz for 72 hours show extensive GlcNAz-Nup62 PLA signals co-localized with nucleus. C. Thiamet G treatment of GlcNAz fed cells show decrease in Nup62-GlcNAz as detected by PLA.

3.5. Conclusions

In this study, we demonstrate the development of a novel assay to detect O-GlcNAc modification in specific proteins in intact mammalian cells. Our assay couples *in situ* PLA with flow cytometry and imaging to quantify levels of O-GlcNAc in specific intracellular proteins. In this study, we have optimized the entire method on the microfluidics chip described in the previous thesis chapter. This offers several advantages including reducing reagent usage and costs and also permits working with a small number of cells. Also, the platform allows users to work with primary cells which are otherwise hard to handle in off chip experiments. More importantly, since the platform is closed and self-contained, it is ideal for working with cells that are infected with BSL3/4 pathogens. It is important to note that while using the chip has advantages, this assay can also be performed off-chip (using a similar protocol) in laboratories that do not have chip set up capabilities. The method we have developed in this study is very rapid and can be completed in a day as opposed to the currently used standard immunoprecipitation assay that takes 3-4 days to complete. Further, since we use intact cells, we can easily detect the sub cellular localization of the O-GlcNAcylated proteins by combining the PLA assay with fluorescence imaging.

In this thesis chapter, we have demonstrated the validity of the assay using a previously known O-GlcNAcylated protein, nup62. Future studies are currently ongoing to look at the dynamic changes in O-GlcNAc levels in signaling proteins in response to cell stimulation. For example, using PLA- flow cytometry, it is possible to quantify changes in O-GlcNAc levels in signaling proteins, such as NFAT and NFkB in response to T-cell receptor (TCR) activation of Jurkat cells. Further, it is also

possible to observe the nuclear vs. cytoplasmic localization of these proteins using PLA-imaging. This can be done on the chip by modifying the chip surface with CD3 and CD28 antibody solution in PBS. These two antibodies together stimulate the TCR pathway thereby activating signaling pathways in T cells. Jurkat cells fed metabolically can be flown into the chip and captured and activated on the chip. Cells are subsequently labeled with click chemistry and antibodies specific to NFAT or NFkB. The proximity ligation assay is performed exactly as described previously in this chapter. Analysis by flow cytometry or imaging enables detection of O-GlcNAcylation levels of these proteins.

The assay developed in this study has many potential applications. As mentioned earlier, it is a simple method to detect O-GlcNAcylation in single intracellular proteins. Further, by multiplexing with site-specific phosphorylation antibodies, it is also possible to use this method to study the dynamic crosstalk or interplay between phosphorylation and O-GlcNAcylation. The method can also be used to study O-GlcNAcylation as a mechanism of host response to pathogens and their virulence factors in both innate and adaptive immunity.

Chapter 4.

Rapid detection of microRNA 155 and CD69 protein at single cell resolution using LNA flow fluorescent *in situ* hybridization (flow-FISH) and rolling circle amplification

4.1. Abstract

microRNAs (miRNAs) are non-coding small RNAs that have cell type-dependent expression and function(*94*). Using an integrated microfluidic based approach, we have developed a flow-FISH method using locked nucleic acid probes and rolling circle amplification to rapidly assess miRNA at single cell resolution using flow cytometry and microscopy. Our microfluidic based flow-FISH method utilizes only 220nL of reagent per experimental condition, and can be multiplexed with protein immunostaining. We demonstrate our method by detecting miR155 and CD69 protein expression in PMA and Ionomycin stimulated Jurkat cells, showing the ability to assess miRNAs in specific cell types identifiable by unique protein markers. The microfluidic LNA flow-FISH method is the first to directly detect miRNA in single cells using flow cytometry, and can be scaled up for bench-scale sample preparation for greater applicability to the scientific community.

4.2. Introduction

Role of microRNA in the immune system

microRNAs or miRNAs are non-coding, small single-stranded RNAs that regulate gene expression in mammalian biological systems, including mammalian immune system(*95, 96*). miRNAs function by directly binding the 3' untranslated regions (UTRs) of specific target mRNAs and recruit the RISC complex to degrade the target mRNA(*97*). The miRNAs are abundant and some are highly conserved across species. The most recent release (18.0) of miRBase - an online repository of miRNA nomenclature, sequence data, annotation and target prediction- contains 18226 mature miRNA products in 168 species(*98*). In humans, over 900 miRNAs have been identified, and each miRNA can potentially repress hundreds of target mRNAs, indicating the importance and complexity of this gene regulation system. The expression of over 100 different miRNAs by cells of the immune system suggests that miRNAs play important roles in the signaling processes that underlie development and function of both innate and adaptive immunity(*99*). For example, the expression of miR17-5p, miR-20a, and miR106a all decrease during the differentiation process from hematopoietic progenitor cells into monocytes(*100*). Expression profiling of adaptive immune T and B cells revealed distinct miRNA patterns in T cell subsets(*101*), and in naïve, germinal centre, and post-germinal centre B cells(*102*). miRNAs have also been implicated in the regulation of the connection between the innate and adaptive immunity by regulating dendritic cell differentiation and antigen uptake(*103, 104*). Since miRNAs functions are dependent on the cell type they are expressed in(*94*), it is clear that in order to properly study

miRNAs in heterogeneous populations of immune cells, it will be necessary to develop a method that can simultaneously identify the cellular subtype and quantitatively assess miRNA levels at single cell resolution.

Several methods exist for the detection of miRNAs. Most miRNA detection methods such as Northern blotting(*25*), oligonucleotide microarrays(*26, 27*), qPCR-based detection miRNAs(*28, 29*), and next generation sequencing(*30*) all require the homogenization of large number of cells and making an averaged miRNA measurement. Population averaged miRNA measurements obscure cell to cell variation and population-specific miRNA differences that are known to be important for miRNA function. To date, only *in situ* hybridization (ISH) using locked nucleic acid (LNA) containing probes(*105, 106*) allows detection of miRNA in intact cells without RNA extraction and amplification. However, LNA- ISH is a labor-intensive and expensive method, and must be used in conjunction with enzymatic signal amplification such as TSA to detect miRNAs. TSA is a peroxidase enzyme based signal amplification method that labels tyrosine residues adjacent to the antibody bound to the oligonucleotide probe, which makes TSA's efficiency dependent not only on peroxidase activity, but also the surrounding amino acid composition.(*107*) While highly effective in certain applications, TSA can be non-specific and poor reproducible. In addition, ISH is a qualitative method, used most frequently for fixed tissue sections and analyzed via microscopy, making it difficult to perform miRNA ISH on non-adherent immune cells. We aim to overcome limitations in existing methodology and use the latest technological advancements to develop a novel single-cell resolution method for miRNA detection at single cell resolution.

We chose miR155 in Jurkat cells as our model system because miR155 is expressed in a variety of immune cell types spanning innate and adaptive spectrum, and exerts different function when expressed in different cells (*108-110*). In dendritic cells, miR155 can negatively regulate the IL-1 signaling pathway(*111, 112*); in T cells, miR155 negatively regulates SOCS1 protein, which leads to the increased levels of interleukin-2, a cytokine necessary for T cell proliferation(*110*); in B cells miR155 down-regulates inositol phosphotase SHIP1(*113*), which leads to the formation of germinal centers and antibody class-switching. In addition to being an important immune regulator, miR155 is also widely recognized as a biomarker for numerous autoimmune diseases(*114, 115*) and cancers of immune origin(*116, 117*). Jurkat cells have long been used as a model cell line for the study of T cell activation(*118*). Jurkat cells produce no detectable miR155 without stimulation, but with double stimulation from phorbol 12-myristate13-acetate (PMA) and Ionomycin, Jurkat cells produce increasing amounts of miR155 as a function of time (figure 4.3.D). The combination of the importance of miR155 with the well characterized Jurkat cell line makes them an ideal model system to develop our assay.

Using flow cytometry with fluorescent *in situ* hybridization, or flow-FISH, was first developed to measure telomere length in clinical samples(*119*), and more recently used for much larger and more abundant mRNAs(*120*). The main challenge in using flow-FISH to detect miRNAs is their small size. At an average of 22 nucleotides, the entire mature miRNA is only a fraction the size of a standard ISH probe. To address this problem, Locked nucleic acid (LNA) analogs with constrained ribose ring can be incorporated into the probe to increase the Tm for better signal to

noise ratio and shorter hybridization time. LNA containing probes are currently widely used for miRNA detection with qPCR and ISH(*121, 122*). We used LNA probes in the development of LNA flow-FISH method that provides fast, quantitative detection of miRNAs using micro flow cytometry and microscopy.

Building upon our group's previous experience with microfluidic cell signaling pathway profiling(*93*) and bacterial rRNA flow-FISH(*57*), we designed a novel 10 chamber microfluidic chip platform that can profile miRNA155 and CD69 at single cell resolution in 10 different experimental conditions using only 220 nL of reagent per condition (figure 4.1.A). Instead of using tyramide signal amplification to visualize the miRNA-LNA probe duplex, rolling circle amplification(RCA) was used to produce a more robust and reliable signal. Along with miR155, the early T cell activation protein CD69 is also upregulated by PMA stimulation(*123*). The PMA and Ionomycin induced CD69 was visualized and quantified along with miR155 in the same Jurkat cells using Quantum Dots. The multiplexed miRNA and protein assay represents the first demonstration of detection of miRNA and protein at single-cell resolution using both microscopy and flow cytometry.

4.3. Materials and Methods:

Cell culture and stimulation

Jurkat cells were purchased from ATCC (TIB-152), and cultured in RPMI media (11875-093, Invitrogen) containing 10% FBS (100-500, Gemini) and 0.5 mg/ml penicillin and streptomycin (15240062, Invitrogen). For stimulation of Jurkat cells, cells were seeded at $1x10^6$/ml for 0, 8, 16, 20, or 24 hours with 10ng/mL PMA (P8139, Sigma) and 1μM Ionomycin (I3909, Sigma). After stimulation, $5x10^5$ cells from each condition were set aside for RNA extraction and RT-PCR, the rest of the cells were fixed with 8% paraformaldehyde (Electron Microscopy Sciences) in PBS for 10 min. Fixed cells were pelleted at 300g for 5 min, and washed twice with PBS.

qRT- PCR

$5x10^5$ cells from each condition were set aside prior to fixation and pelleted at 300g for 5 min and washed 2x with PBS. Total RNA was extracted using the RNeasy kit from Qiagen according to manufacturer's instructions. The extracted RNA was quantified using a Nanodrop 2000, and 100ng of RNA was used to generate cDNA using the miScript II RT kit (Qiagen). All steps were performed according to manufacturer's instructions. 100ng of cDNA from each condition was subsequently used in miScript hsa-mir-155 primer assay (Sanger accession: MI0000681, Qiagen), normalized to positive control SNORD61 (Qiagen). Expression level of miRNA155 was analyzed using the $2^{-\Delta\Delta Ct}$ method. SNORD61 served as positive control for normalization. miR155 level at 0 h served as basal level, and miR155 in PMA and Ionomycin treated samples are expressed as fold changes compared with 0h.

Microfluidic chip design and platform setup

The ten chamber microfluidic chip was designed in-house using AutoCAD 2010 (Autodesk Inc., San Rafael, CA), photomasks were generated at Photo Sciences (Torrence, CA), and quartz microfluidic devices were fabricated by Caliper Life Sciences (Hopkinton, MA). An array of fourteen holes 500 μm in diameter, seven on each side, provided for fluid inlet. All subsequent steps in chip packaging and details of the chip platform are as previously described(*93*). Detailed photos of the platform is shown in supplemental figure 4.2.

Microchip surface treatment with Cell-Tak™

The novel planar microfluidic cell preparation chip in this study contains ten horizontal fluidically isolatable microchannel series with the dimensions of w = 200 μm width, d = 30 μm depth, L = 72 mm, each holding up to 2000 macrophages and 220 nL of fluid volume. The 10 channel microchip was cleaned with 10% bleach in filtered DI water for 15 min, followed by flushing with DI to wash off all residual bleach. To make the Cell-Tak™ (354240, BD Biosciences) solution, combine 15μl Cell-Tak™ with 575μl 0.1M sodium bicarbonate pH 8.0, followed by adding 10μl of 1N NaOH immediately prior to adsorption onto chip. Flow Cell-Tak™ solution into chip for at least 15min, followed by PBS flush for 5 min. Fixed Jurkat cells can now be captured on the microchannel surface for flow ISH.

On-chip LNA *in situ* hybridization

The miR155 (/5DigN/ACCCCTATCACGATTAGCATTAA/3Dig_N/) and scrambled (/5DigN/GTGTAACACGTCTATACGCCCA/3DIG_N/) LNA double DIG labeled probes were purchased from Exiqon. Fixed Jurkat cells were loaded into the chip as shown in figure 9A. Cells are allowed to settle and adhere to the micro channel

surface for 30min. During the settling time, the following solutions were made fresh: solution 1 (0.13 M 1-methylimidazole, 300mM NaCl, pH 8.0, adjusted with HCl), EDC solution (0.16M EDC in solution 1, adjusted to pH 8.0), hybridization buffer (50% formamide, 2x SSC, 50μg/ml yeast tRNA, 50μg/ml salmon sperm, 50mM NaPi). To permeabilize the Jurkat cells, 0.25% Triton-X 100 in TBS was flown into all chambers for 10 min, followed by 5 min wash with solution 1. After incubation with solution 1, solution 2 was flown into all chambers and cells were incubated for 20 min at RT in solution 2, followed by a 5 min wash with TBS. The cells were then pre-hybridized for 30min at 62°C in hybridization buffer pre-warmed to 65°C. All LNA probes were used at 10 pmol/25μl hybridization buffer, and flown into pre-determined chambers. The hybridization with LNA probes were performed at 80°C for 90s, followed by 90 min at 62°C. Following the LNA probe hybridization, all chambers were washed with 2x SSC + 50% Formamide at 65°C for 10min (flow 5min, stop 5min), then washed with 1X SSC for 20min (flow 5min, stop 15min) at RT, and finally washed with 0.1X SSC for 20min (flow 5min, stop 15min) at RT.

Signal amplification using rolling circle amplification

To amplify the LNA bound miRNA signals, the FITC Duolink mouse PLUS (92001-0030) and mouse MINUS (92004-0030) probes and detection kit (92014-0030) from Olink Biosciences were used to perform rolling circle amplification of miRNA signals. After *in situ* hybridization, the cells were blocked with 2% BSA for 30min at 37°C, followed by incubation with anti-DIG antibody (11333062910, Roche) at 1:50 for 1h at 37°C. Cells were then washed with TBST for 5min. The Duolink mouse PLUS and MINUS probes were diluted at 1:5 (20μl PLUS + 20μl MINUS + 60μl

dilution buffer from kit), flow into all chambers, and incubated for 1h at 37°C. After probe incubation, all chambers were washed for 5 min with TBST. The ligation and amplification steps were done according to manufacturer's instructions, using only 1 reaction volume for all 10 chambers.

CD69 protein immunostaining multiplexed with LNA flow-FISH

To multiplex protein immunostaining with LNA flow-FISH, Jurkat cells were stained with anti-CD69-biotin antibody at 1:100 (13-0699-80, eBioscience) in PBS for 30min at RT prior to permeabilization with 0.25% Triton. A solution of CD69 antibody was flown into all chambers, flow was then stopped for 30 min for the incubation. All chambers were washed with TBS with 0.05% Tween for 5 min, followed by 30min incubation with a 1:2000 solution of Qdot 705 streptavidin conjugate (Q10161MP, Invitrogen) in PBS. Following Qdot 705 Streptavidin incubation, all chambers were washed with TBST for 5 min. All chambers were then washed with TBST for 5min. The *in situ* hybridization procedure continues from this point on at the permeabilization step.

Microscopy and image analysis

Prior to imaging, the cells were incubated with Hoechst stain (33342, Pierce) in PBS for 10min, followed by 10 min wash in PBS. Epi-fluorescent images were captured at 60X magnification on an Olympus IX-71 microscope equipped with GFP, Texas Red, DAPI filters and Hamamatsu ORCA-R2 cooled CCD camera controlled via micro-manager free software. Images were artificially colored and overlaid in ImageJ.

On-chip laser induced fluorescence and flow cytometry

The on-chip flow cytometry was performed as previously described (*93*). Briefly, a 20-mW 488-nm solid-state laser (Cyan; Newport, Irvine, CA) was used for excitation. Forward scattering detected through an optical fiber (JTFSH 600 μm core; Polymicro Technologies, Phoenix, AZ) and a bandpass filter with blocker (488NB2.6; Omega, Brattleboro, VT) connected to a photomultiplier (H5784-20; Hamamatsu, Bridgewater, NJ). Laser-induced fluorescence emission is split (600DCXR longpass filter; Chroma, Rockingham, VT) into a yellow channel (FL2-H: 585/42m bandpass filter), and following a second dichroic (750DCXR longpass filter; Chroma) into a red channel (FL3-H: 655LP longpass filter) and a far-red channel (FL4-H) before being detected by three photomultipliers. All four photomultiplier voltages (488-nm scatter, yellow, red and far-red) are recorded by a data acquisition module (NI 9401; National Instruments, Austin, TX). After on-chip sample preparation, cells were detached via proteolytic cleavage using 100ug/mL elastase (I.U.B.: 3.4.21.36, Worthington), and hydrodynamically focused for on-chip flow cytometry. In-house software for data collection was scripted using LabVIEW. The scatter and fluorescence captured by each PMT module was collected using a computer equipped with National Instruments data acquisition module, and the data was further analyzed using the Peak Finder application in LabVIEW. The text files containing peak values for each scatter and fluorescence measurement were then imported into Excel, and histograms for each experimental condition were generated and overlaid.

4.4. Results and discussion:

To develop and optimize the detection of miRNA155 at single cell resolution, we used a novel 10 chamber microfluidic chip for sample preparation and on-chip flow cytometry shown in figure 4.1.A. The microfluidic chip has fluidically isolatable cell holding chambers numbered 1 through 10, each capable of holding up to 2000 cells per condition. After sample preparation, the cells in the chambers can be detached using proteolytic cleavage, and driven by positive pressure to the center of the chip where they are hydrodynamically focused (figure 4.1.B) and interrogated using micro-flow cytometry on our in-house setup (figure 4.2). Prior to cell loading, the microchannel surfaces are pre-coated with Cell Tak™ solution to facilitate capture of non-adherent Jurkat cells. Once the cells are loaded into the chambers, double DIG labeled LNA probe against miR155 is hybridized to mature miR155 molecules inside the Jurkat cells. The miRNA155 signals are then amplified using a method depicted in figure 8C. The LNA probe hybridizes with miR155 inside the Jurkat cell, and a monoclonal antibody (mAb) is used to bind the DIG labels at both ends of the LNA probe. A pair of PLA probes(one positive, one negative) composed of antibody tethered to oligonucleotides, are used to bind to the anti-DIG antibody. After binding to the anti-DIG antibody, the two probes are ligated to additional oligonucleotides to form a circular template for subsequent rolling circle amplification with phi29 polymerase. Resultant single-stranded concatemers are detected with fluorescent labeled oligonucleotide probes directed against short sequences encoded in the template. The signals can be visualized as fluorescent dots in the cell (figure 4.4.A), as well as detected via flow cytometry. Jurkat cells stimulated with PMA and

Ionomycin for 0, 8, 16, 20, and 24 h were loaded in duplicate into the 10 chamber chip (figure 4.3.A). The top 5 chambers were hybridized with double DIG labeled miR155 LNA probe, and the bottom 5 chambers were hybridized with double DIG labeled scrambled probe as negative control. The RCA amplified miR155 fluorescence was quantified using on-chip flow cytometry and the fluorescence histograms are overlaid and shown in figure 4.3.B, and the median values from each condition was plotted as a bar graph shown in figure 4.3.C. Both the overlay and the bar graph of median values shows incremental increase in the miR155 production of Jurkat cells under stimulation with PMA and Ionomycin, while the scrambled control fluorescence remained low throughout the time course. The miRNA flow-FISH results were verified using RT-qPCR using cells that were taken from the same sample prior to fixation for flow-FISH analysis (figure 4.3.D). The experiment shown in figure 4.2 is representative of 3 biological replicates. Both LNA flow-FISH and qPCR shows the same trend of miR155 increasing with longer PMA and Ionomycin stimulation.

To detect miRNAs and CD69 in the same Jurkat cells, staining with anti-CD69 antibody was done prior to fixation with EDC. Figure 4.4 shows representative images of Jurkat cells with miR155 as green dots, CD69 protein in red, and nucleus in blue. At time 0, no CD69 and almost no miR155 can be seen. The size and intensity of green miR155 dots increase as duration of stimulation increases. CD69 is an early T cell activation marker, and it also increases with PMA and Ionomycin stimulation. After microscopy, the same cells were detached and analyzed using flow cytometry, the median fluorescence values from miR155 and CD69 are plotted in the same graph

(figure 4.4.B), showing increase of both miR155 and CD69 with increased duration of PMA and Ionomycin stimulation.

The miRNA flow-FISH assay we developed uses a novel combination of LNA probes with RCA signal amplification for a robust miRNA signal that can be quantified by flow cytometry as well as visualized using microscopy. The biggest advantage of the flow-FISH method is that both qualitative images and quantitative miRNA and protein measurements at single cell resolution can be obtained in less than 10 hours. The higher Tm of the LNA containing probes increase specificity while drastically reduce the hybridization time from days to 90 min. The analysis with flow cytometry can be performed in minutes, compared to the days and weeks needed to quantify signal using microscopy. Secondly, unlike established small RNA FISH methods that utilize tyramide signal amplification, RCA amplification uses two antibody tethered oligonucleotide probes that can be ligated to form a circle when bound to the DIG labels on the ends of the LNA probe (Fig.4.1.B). Since only the ligated circular DNA template can be amplified by the RCA polymerase, RCA signal amplification is not dependent on the environment the miRNA is residing in, making RCA a superior signal amplification method to TSA. An added benefit to using RCA is that the miR155 signal can be visualized as distinct fluorescent dots and can be quantified using microscopy alone if flow cytometry is not available. For multiplexing of protein immunostaining with miRNA flow-FISH, special consideration had to be made. The high Tm of LNA containing probes provides superior specificity and rapid hybridization when used to detect small miRNAs, but the high hybridization temperature can reverse formaldehyde fixation, and miRNAs

can be washed away. A second fixation step using 1-ehty-3-(3-dimethyl-aminopropyl) carbodiimide or EDC must be used in addition to formaldehyde fixation to irreversibly cross-link the miRNA to the neighboring amino acid residues(*105*). The activation of phosphates by EDC is shown in figure 4.5. The EDC fixation step retains miRNAs inside the cell, but destroys protein epitopes as well as protein based fluorephores such as phycoerytherin. Hence, we chose quantum dots for multiplexing of protein detection with LNA flow-FISH because they are not inert to EDC fixation.

The multiplexed protein and LNA flow-FISH method for miRNAs can be used to profile miRNA levels in individual cells from mixed populations such as PBMCs. Each immune subset can be identified using cell-type specific protein markers, and their miRNAs can be assessed in simultaneously. Complex primary blood samples from patients with known miRNA dysregulation (lupus, leukemia) can be profiled rapidly, and the miRNA levels in subset of cells can be more accurately profiled using our microfluidic platform. Of course, if sample and reagent are not limiting, bench-scale preparations can be done as well. Another important potential use of this method is to develop direct functional assays for miRNAs. To date, functional target validation of miRNAs are limited to bioinformatic predictions and in vitro assays that express the miRNA sequence on plasmids that are transfected into reporter cell lines that are ultimately reliant on population averaged methods such as qPCR or Western blotting(*124*). With our miRNA flow-FISH method, multiplexing the detection of miRNA and their protein target in the same cell provides a direct way to study miRNA effects on signaling *in vivo*. Such a functional assay used in combination with our microfluidic platform can open the door to studying miRNA

and their effects on signal transduction in rare and primary cells that have been beyond the reach of existing technology.

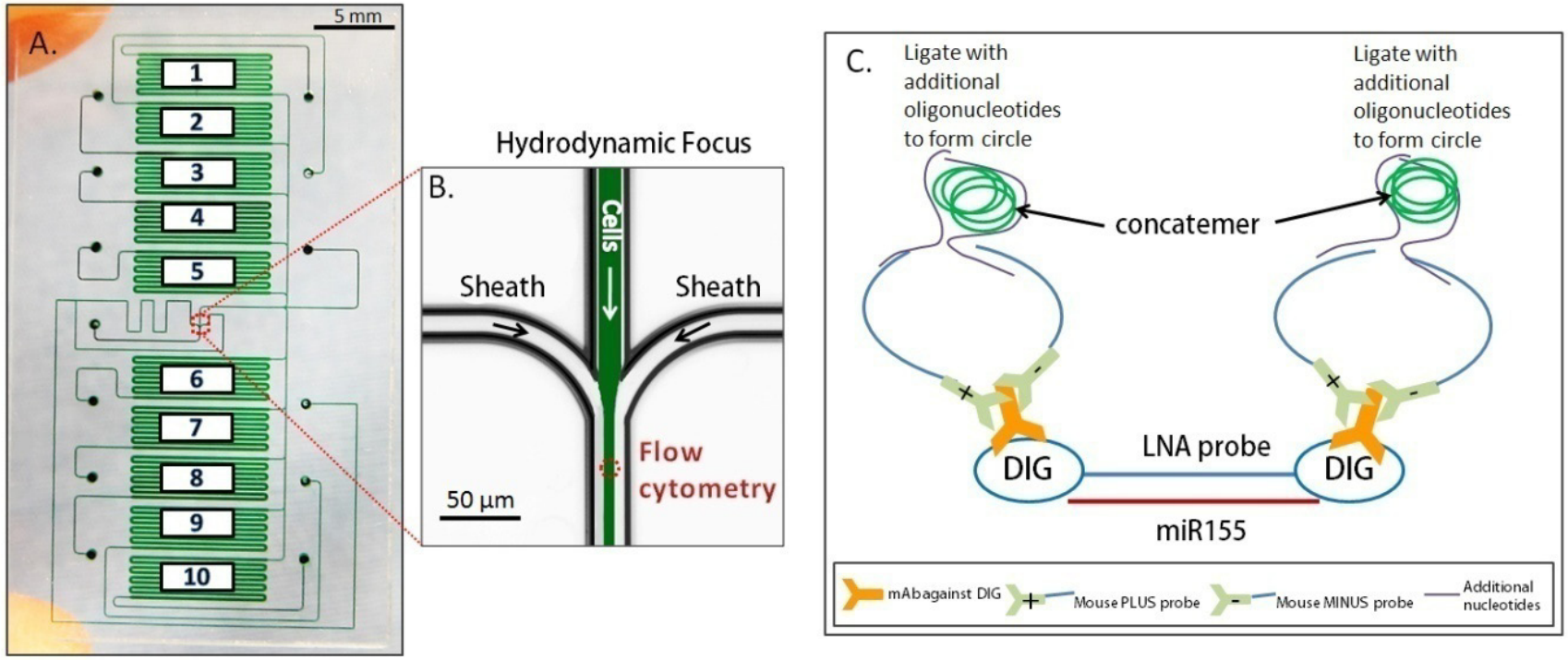

Figure 4.1. A. 10 chamber microfluidic chip. Cells prepared in each of the holding chambers can be detached and driven to the center of the chip shown in B, for hydrodynamic focus and flow cytometry. The signal from miRNA155 hybridized to the LNA probe is amplified using a method depicted in C. The DIG label on both ends of the LNA probe is recognized by mAb, and two RCA probes (+ and -) bind to each anti-DIG mAb and are ligated to two more oligonucleotides to form circular templates for rolling circle amplification. The resultant fluorescent concatemers can be visualized using microscopy as well as measured using flow cytometry.

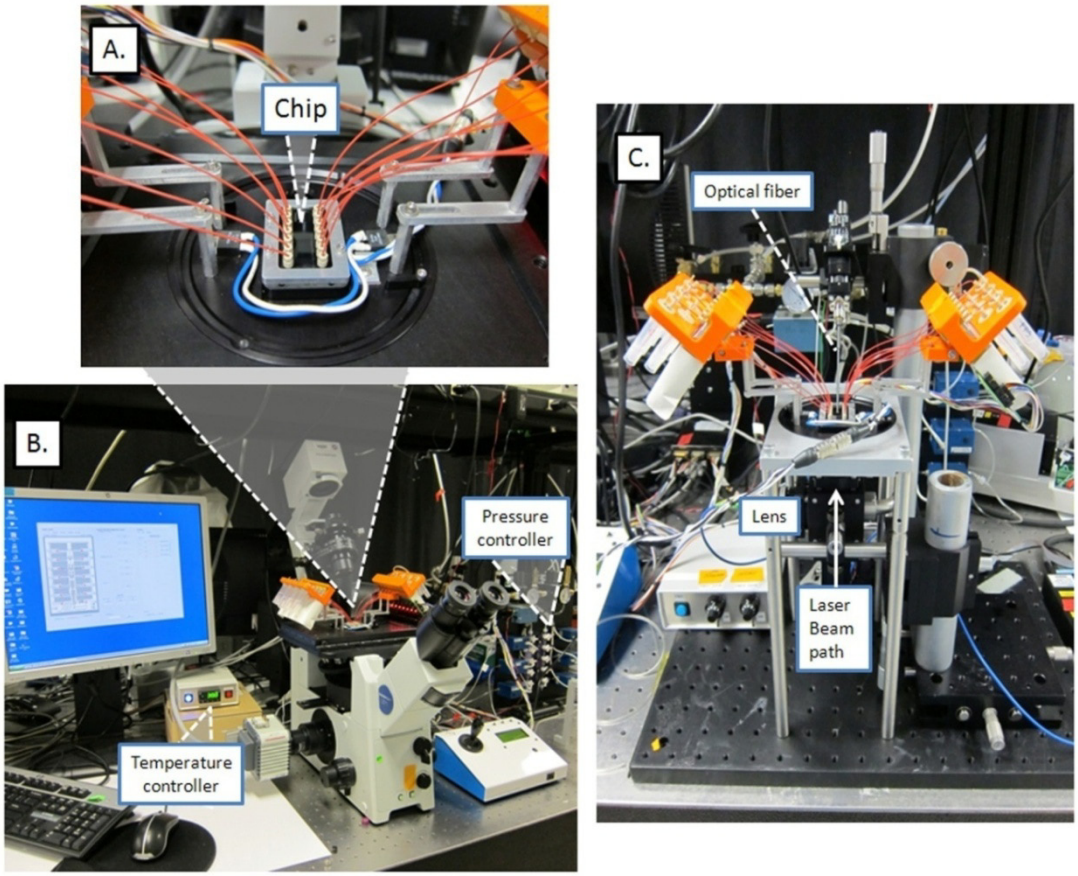

Figure 4.2. Microfluidic platform. The planar microfluidic chip sits in a manifold designed in-house (A). Tubing connect valves and reagent reservoires to the inlets on the microfluid chip. B. The manifold is retrofitted to a commercial Olympus IX71 microscope. In-house designed software allows the experimenter to control the pressure, temperature, and valves by programming the each step of the experiment to run automatically. After sample preparation, the manifold is moved to the micro flow cytometer setup shown in C, and on-chip flow cytometry is performed. The optical fiber is positioned on top of the chip, and aligned to the hydrodynamically focused path of the cells. The laser is applied from the bottom of the chip, and the voltages from the laser induced fluorescence in the passing cells are recorded by the PMTs situlated underneath the chip.

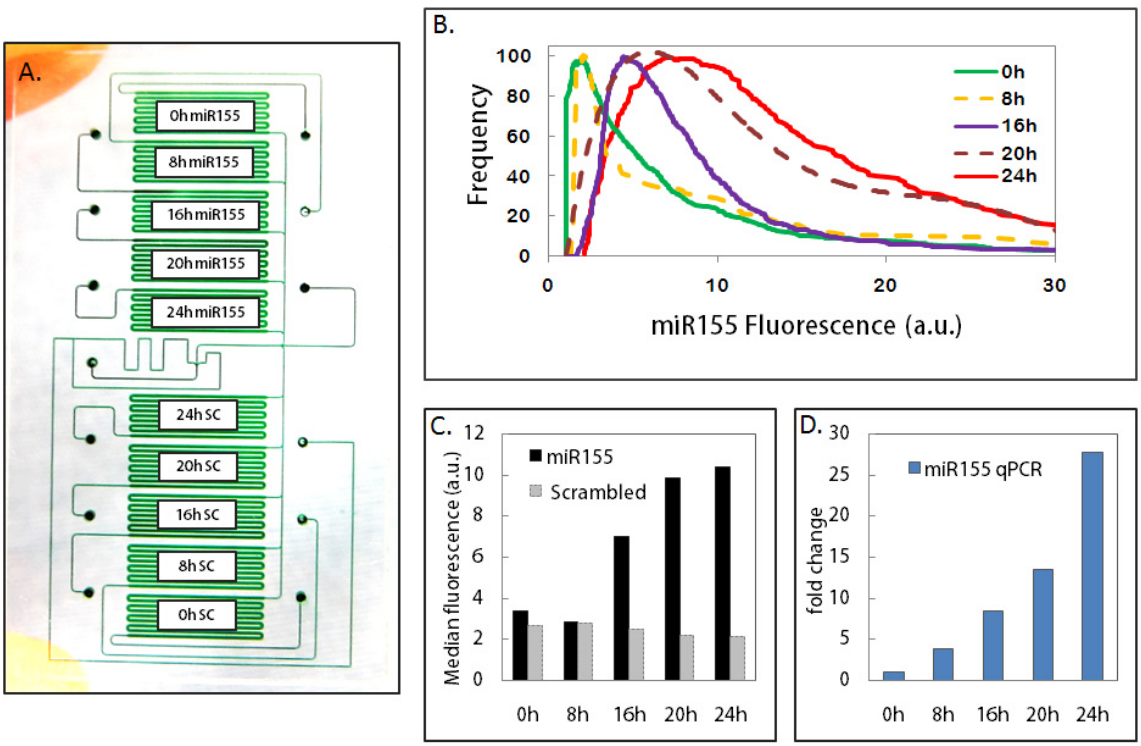

Figure 4.3. Jurkat cells stimulated with PMA and Ionomycin for 0, 8, 16, 20, and 24h were loaded in duplicate into the 10 channel chip as shown in A. B. miR155 fluorescence assessed using on-chip flow cytometry. C. Median values of the miR155 fluorescence compared to scrambled negative control. D. RT-qPCR of the same cells used for the LNA flow-FISH.

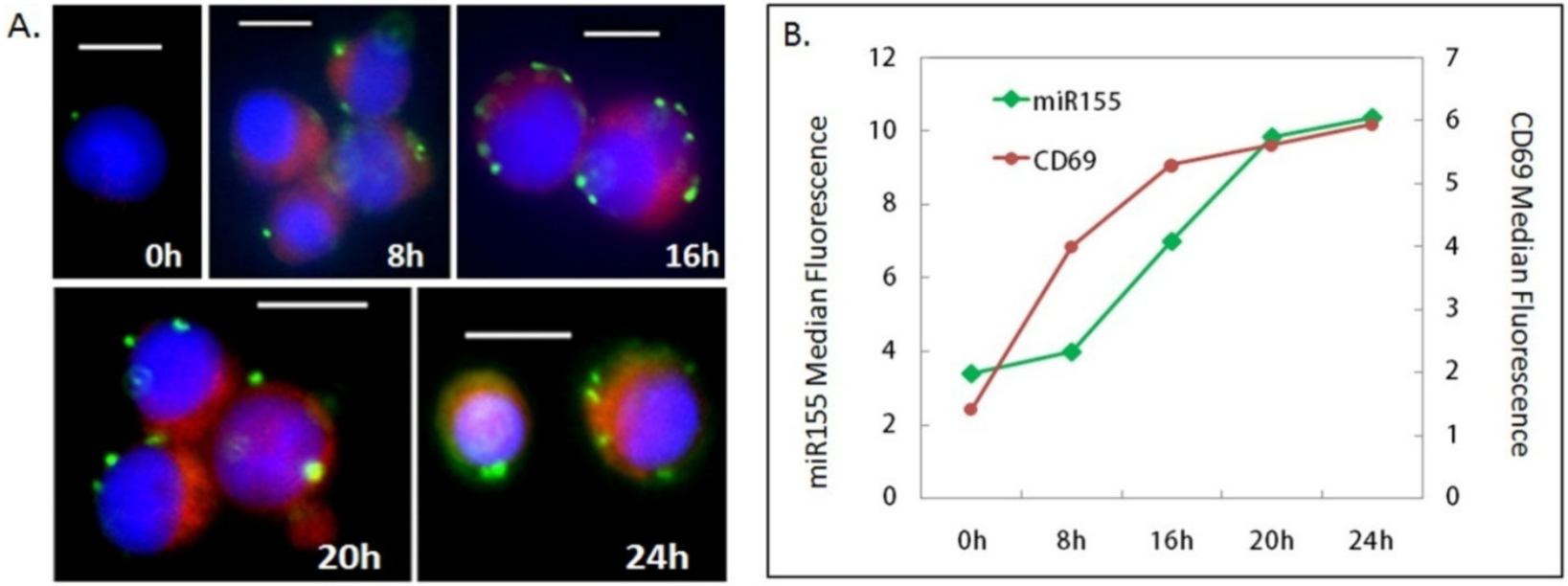

Figure 4.4 Multiplexed detection of miR155 and CD69 protein. A. Image panel Jurkat cells showing RCA amplified miR155 signal as green dots in the cytosol, CD69 proteins stained with Qdot705 are red, and the nucleus is shown in blue. B. Median values of miR155 fluorescence and CD69-Qdot705 fluorescence from the same cells.

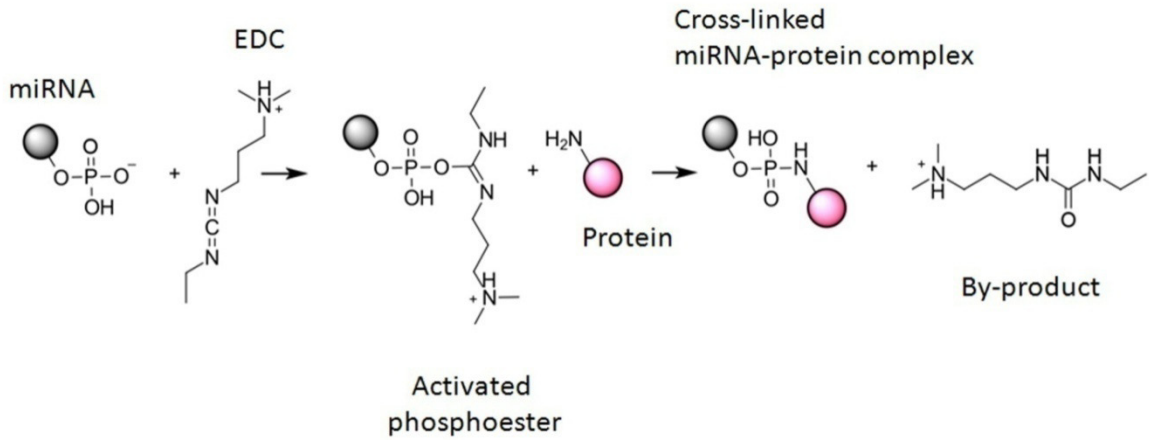

Figure 4.5 EDC fixation of miRNA to surrounding proteins. The 5' phosphate of miRNA are activated by EDC to form an intermediate that is crosslinked to neighboring amino groups of proteins. The fixation with EDC allows irreversible crosslinking to tether miRNAs inside the cells during the high temperature hybridization with LNA containing probes.

4.5. Conclusion

We have developed a novel method for multiplexed detection of miRNA and proteins at single cell resolution using both flow cytometry and microscopy, performed in a novel 10 chamber microfluidic chip platform. The increased number of chambers from our previously published chips(*17, 93*) provides the necessary throughput for this assay development and future biological experiments. The biggest advantage of the new method is the capability to multiplex detection of miRNA and proteins in the same intact cell. Correlations between miRNA and proteins whose abundance they regulate, can potentially be directly addressed without the need for *in vitro* expression systems. The experimental conditions optimized on the microfluidic chip can easily be scaled up for bench scale preparations for those that do not have microfluidics capabilities.

Chapter 5.

Conclusion and Future Directions

The focus of this thesis is the development of a novel microfluidic device and accompanying cell based assays that interrogate various aspects of immune cell signaling pathways. Chapter 1 provides a comprehensive background on single-cell analysis techniques and also discusses the microfluidic device that can integrate multi-parameter single-cell quantitative analysis. In chapter 2, events beginning with receptor activation to cytokine production, spanning the entire macrophage TLR4 pathway, were profiled using one microfluidic experiment, generating data later used for mathematical modeling. The novelty lies in the integration on-chip preparation of four different assays in one microfluidic platform, which is made possible by the valves and pressure controllers that move cells and fluid through the chip without introducing cell loss and cross contamination. The device combines on chip sample preparation and assays with multi-parameter flow cytometry and fluorescence imaging that allows the analysis of multiple fluorescent protein species from the same sample prepared on the chip. In the subsequent chapters, the utility of the microfluidic device has been extended to develop additional methods that enable detection of cellular levels of post-transcriptional and post-translational regulators of cell signaling. In chapter 3, a novel assay to detect dynamic glycosylation (or O-GlcNAc modification) of proteins is developed for use on the microfluidic platform. The O-GlcNAc modification, which is similar to Ser/Thr phosphorylation of signaling proteins, is an important PTM involved in regulation of cell signaling, but has been largely neglected by the cell signaling community due to the lack of reagents to rapidly and easily detect specific O-GlcNAcylated proteins. The novel assay presented in chapter 3 is the first of its kind to combine metabolic labeling of

bioorthogonal probes with proximity ligation assay, two commercially available reagents that can be used to detect O-GlcNAc levels on specific proteins of interest. In chapter 4, a novel method for the detection of miRNA in single cells is developed using LNA flow-FISH method using the same microfluidics platform. It is the first such method that exploits the rapid speed and throughput of flow cytometry to analyze miRNA at single-cell resolution. An added benefit of the LNA flow-FISH method is the capability to multiplex with protein immunostaining in the same cells. The concurrent detection of miRNA and proteins in the same intact cell opens the possibility to profile miRNAs in heterogeneous immune subsets identified by cell specific markers as a diagnostic, or possibly developing a direct functional assay that can measure target protein levels of miRNAs at single cell resolution.

Perhaps the most important advantage of microfluidic single-cell assays is that on-chip sample preparation and analysis can integrate methods that are otherwise incompatible without a chip. This point is best demonstrated by the development of the two novel assays in chapters 3 and 4. In the miniaturized environment of the microchannels, cells are spread across the bottom of the channel in a monolayer, giving each cell increased exposure to the reagents in the channel, and thereby increasing the labeling efficiency of the molecular probes. Also, with the elimination of centrifugation steps, better permeabilization was achieved, and minimal cell loss (by lysis) resulted in increased data collection. Other advantage of microfluidic assays is their minimal requirement for sample and reagents. With a ~95% reduction in reagent, it's possible to develop and optimize assays using the newest, most cutting-edge reagents without the concern for cost. In addition, in cases where

reagents or samples are limited, such as those with labor-intensive custom generated reagents or precious primary cells, microfluidics devices become not just a convenience, but a necessity.

Future applications

The purpose of this Ph.D. work is an attempt at bridging a gap between technology development and its implementation in Biological sciences, where a microfluidic platform is improved and applied to solve some technical problems that are difficult, if not impossible to address using existing technology. The most obvious future application for the technologies developed in this thesis is in basic research into cell signaling of primary mammalian cells. For example, mouse geneticists often require the lymphocytes of an entire animal to generate one data point when preparing samples on the bench, followed by analysis using a commercial flow cytometer. Microfluidic sample preparation detailed in this thesis requires only 10,000-25,000 cells to generate 10 different data points, making it possible to profile entire pathways in extremely limited samples, without the need to pool tissue from different animals. The two novel assays to detect dynamic O-GlcNAcylated proteins and miRNAs in intact cells can be multiplexed with signaling protein pathway profiling to provide a more complete and accurate picture of how cell signaling is regulated by post-transciptional and post-translational regulators. Other limited samples include clinical samples from neonates or very ill patients, rare immune subsets, and biopsies, where the small sample requirement for profiling an entire signaling pathway can really make an impact on the speed which progress can be made.

Another important use for the microfluidic platform and assays developed here are for the use in studying host/pathogen interactions of BSL3/4 infectious agents for both public health and biodefense applications. The small footprint of the platform and its total containment capability minimizes handling time and possible exposure to infectious agents. Ideally, a microfluidic station can be set up inside a BSL3/4 facility, and host/pathogen interaction and host response signaling pathways can be profiled with maximum efficiency and minimal risk to the work force and public. Alternatively, engineering efforts can be made to make the platform and its accompanying assays portable, so that sophisticated cell based assays can be conducted in the field, and greatly speed the identification of infectious agents and the correct therapeutic remedy for those exposed.

Aside from the above mentioned applications basic research and biodefense, there are potential for use in Point-of-Care (POC) and personalized biomarker markets. To date, there is no cell based POC device that enables the rapid profiling of signaling pathways in live cells taken from the patient. Our device, along with a set of optimized assays, can be used to profile known pathways that underlie medical conditions, such as the TLR9 pathway defects in the B cells of common variable immune deficiency (CVID) patients, and provide rapid diagnosis that lead to early intervention and improved quality of life for patients. Aside from diagnostics, miRNA and O-GlcNAcylation serve as potential biomarkers for various diseases ranging from inflammation to cancer. The rapid profiling of miRNAs and O-GlcNAcylation can be done with minimally invasive finger prick, and the analysis can then be automated at the doctor's office. Cell-based POC devices can potentially

lower the costs of diagnostic tests and improve the efficiency of medical diagnosis and monitoring of patient progress.

Towards these future applications, our group is currently conducting proof-of-concept studies in the use of this microfluidic platform to study virus/host interactions, and profile signaling pathways in primary immune cells. The most crucial development however, will be the forging of meaningful collaboration between the engineers and biologists to bring some real biological problems to be solved on the microfluidic platform. Hopefully, the demonstrations of the microfluidic platform's versatility presented in this thesis will gather enough interest from the Biological community to forge just such fruitful collaborations.

Bibliography:

1. Wu, M., and Singh, A. K. (2012) Single-cell protein analysis, *Current opinion in biotechnology 23*, 83-88.
2. d'Hennezel, E., Yurchenko, E., Sgouroudis, E., Hay, V., and Piccirillo, C. A. Single-cell analysis of the human T regulatory population uncovers functional heterogeneity and instability within FOXP3+ cells, *J Immunol 186*, 6788-6797.
3. Ghoreschi, K., Laurence, A., Yang, X. P., Hirahara, K., and O'Shea, J. J. T helper 17 cell heterogeneity and pathogenicity in autoimmune disease, *Trends Immunol*.
4. Yamazaki, S., and Nakauchi, H. (2009) Insights into signaling and function of hematopoietic stem cells at the single-cell level, *Curr Opin Hematol 16*, 255-258.
5. Curtis, M. G., Walker, B., and Denny, T. N. Flow cytometric methods for prenatal and neonatal diagnosis, *J Immunol Methods 363*, 198-209.
6. Harrison, D. K., Voss, C., Vollmar, H. S., Koutsiaris, A. G., and Newton, D. J. (1998) Response of muscle oxygen saturation to exercise, measured with near infrared spectrophotometry in patients with peripheral vascular disease, *Adv Exp Med Biol 454*, 45-52.
7. Snijder, B., Sacher, R., Ramo, P., Damm, E. M., Liberali, P., and Pelkmans, L. (2009) Population context determines cell-to-cell variability in endocytosis and virus infection, *Nature 461*, 520-523.

8. Goaillard, J. M., Taylor, A. L., Schulz, D. J., and Marder, E. (2009) Functional consequences of animal-to-animal variation in circuit parameters, *Nat Neurosci 12*, 1424-1430.

9. De Rosa, S. C., Herzenberg, L. A., and Roederer, M. (2001) 11-color, 13-parameter flow cytometry: identification of human naive T cells by phenotype, function, and T-cell receptor diversity, *Nature medicine 7*, 245-248.

10. Perfetto, S. P., Chattopadhyay, P. K., and Roederer, M. (2004) Seventeen-colour flow cytometry: unravelling the immune system, *Nature reviews. Immunology 4*, 648-655.

11. Perez, O. D., and Nolan, G. P. (2002) Simultaneous measurement of multiple active kinase states using polychromatic flow cytometry, *Nature biotechnology 20*, 155-162.

12. Sachs, K., Perez, O., Pe'er, D., Lauffenburger, D. A., and Nolan, G. P. (2005) Causal protein-signaling networks derived from multiparameter single-cell data, *Science 308*, 523-529.

13. Irish, J. M., Hovland, R., Krutzik, P. O., Perez, O. D., Bruserud, O., Gjertsen, B. T., and Nolan, G. P. (2004) Single cell profiling of potentiated phospho-protein networks in cancer cells, *Cell 118*, 217-228.

14. Karlsson, A. C., Martin, J. N., Younger, S. R., Bredt, B. M., Epling, L., Ronquillo, R., Varma, A., Deeks, S. G., McCune, J. M., Nixon, D. F., and Sinclair, E. (2003) Comparison of the ELISPOT and cytokine flow cytometry assays for the enumeration of antigen-specific T cells, *J Immunol Methods 283*, 141-153.

15. Henriksen, M., Miller, B., Newmark, J., Al-Kofahi, Y., and Holden, E. Laser scanning cytometry and its applications: a pioneering technology in the field of quantitative imaging cytometry, *Methods Cell Biol 102*, 159-205.

16. Lindstrom, S., and Andersson-Svahn, H. (2010) Overview of single-cell analyses: microdevices and applications, *Lab on a chip 10*, 3363-3372.

17. Srivastava, N., Brennan, J. S., Renzi, R. F., Wu, M., Branda, S. S., Singh, A. K., and Herr, A. E. (2009) Fully integrated microfluidic platform enabling automated phosphoprofiling of macrophage response, *Analytical chemistry 81*, 3261-3269.

18. Venable, A., Mitalipova, M., Lyons, I., Jones, K., Shin, S., Pierce, M., and Stice, S. (2005) Lectin binding profiles of SSEA-4 enriched, pluripotent human embryonic stem cell surfaces, *BMC developmental biology 5*, 15.

19. Boyce, M., and Bertozzi, C. R. (2011) Bringing chemistry to life, *Nature methods 8*, 638-642.

20. Dehnert, K. W., Beahm, B. J., Huynh, T. T., Baskin, J. M., Laughlin, S. T., Wang, W., Wu, P., Amacher, S. L., and Bertozzi, C. R. Metabolic labeling of fucosylated glycans in developing zebrafish, *ACS Chem Biol 6*, 547-552.

21. Cohen, A. S., Dubikovskaya, E. A., Rush, J. S., and Bertozzi, C. R. Real-time bioluminescence imaging of glycans on live cells, *J Am Chem Soc 132*, 8563-8565.

22. Czech, B., and Hannon, G. J. (2011) Small RNA sorting: matchmaking for Argonautes, *Nature reviews. Genetics 12*, 19-31.

23. O'Neill, L. A., Sheedy, F. J., and McCoy, C. E. (2011) MicroRNAs: the fine-tuners of Toll-like receptor signalling, *Nature reviews. Immunology 11*, 163-175.

24. Sheedy, F. J., Palsson-McDermott, E., Hennessy, E. J., Martin, C., O'Leary, J. J., Ruan, Q., Johnson, D. S., Chen, Y., and O'Neill, L. A. (2010) Negative regulation of TLR4 via targeting of the proinflammatory tumor suppressor PDCD4 by the microRNA miR-21, *Nature immunology 11*, 141-147.

25. Valoczi, A., Hornyik, C., Varga, N., Burgyan, J., Kauppinen, S., and Havelda, Z. (2004) Sensitive and specific detection of microRNAs by northern blot analysis using LNA-modified oligonucleotide probes, *Nucleic acids research 32*, e175.

26. Castoldi, M., Schmidt, S., Benes, V., Noerholm, M., Kulozik, A. E., Hentze, M. W., and Muckenthaler, M. U. (2006) A sensitive array for microRNA expression profiling (miChip) based on locked nucleic acids (LNA), *RNA 12*, 913-920.

27. Thomson, J. M., Parker, J., Perou, C. M., and Hammond, S. M. (2004) A custom microarray platform for analysis of microRNA gene expression, *Nature methods 1*, 47-53.

28. Duncan, D. D., Eshoo, M., Esau, C., Freier, S. M., and Lollo, B. A. (2006) Absolute quantitation of microRNAs with a PCR-based assay, *Analytical biochemistry 359*, 268-270.

29. Raymond, C. K., Roberts, B. S., Garrett-Engele, P., Lim, L. P., and Johnson, J. M. (2005) Simple, quantitative primer-extension PCR assay for direct monitoring of microRNAs and short-interfering RNAs, *RNA 11*, 1737-1744.

30. Xu, G., Fewell, C., Taylor, C., Deng, N., Hedges, D., Wang, X., Zhang, K., Lacey, M., Zhang, H., Yin, Q., Cameron, J., Lin, Z., Zhu, D., and Flemington, E. K. (2010) Transcriptome and targetome analysis in MIR155 expressing cells using RNA-seq, *RNA 16*, 1610-1622.

31. Spiller, D. G., Wood, C. D., Rand, D. A., and White, M. R. (2010) Measurement of single-cell dynamics, *Nature 465*, 736-745.

32. Kurien, B. T., Dorri, Y., Dillon, S., Dsouza, A., and Scofield, R. H. (2011) An overview of Western blotting for determining antibody specificities for immunohistochemistry, *Methods Mol Biol 717*, 55-67.

33. Reen, D. J. (1994) Enzyme-linked immunosorbent assay (ELISA), *Methods Mol Biol 32*, 461-466.

34. Wolf-Yadlin, A., Sevecka, M., and MacBeath, G. (2009) Dissecting protein function and signaling using protein microarrays, *Current opinion in chemical biology 13*, 398-405.

35. Sung, M. H., and McNally, J. G. (2011) Live cell imaging and systems biology, *Wiley interdisciplinary reviews. Systems biology and medicine 3*, 167-182.

36. Suni, M. A., and Maino, V. C. (2011) Flow cytometric analysis of cell signaling proteins, *Methods Mol Biol 717*, 155-169.

37. Spencer, S. L., Gaudet, S., Albeck, J. G., Burke, J. M., and Sorger, P. K. (2009) Non-genetic origins of cell-to-cell variability in TRAIL-induced apoptosis, *Nature 459*, 428-432.

38. Chen, B. S., and Wu, S. N. (2011) Functional role of the activity of ATP-sensitive potassium channels in electrical behavior of hippocampal neurons: experimental and theoretical studies, *Journal of theoretical biology 272*, 16-25.

39. Batchelor, E., Loewer, A., and Lahav, G. (2009) The ups and downs of p53: understanding protein dynamics in single cells, *Nat Rev Cancer 9*, 371-377.

40. Tay, S., Hughey, J. J., Lee, T. K., Lipniacki, T., Quake, S. R., and Covert, M. W. (2010) Single-cell NF-kappaB dynamics reveal digital activation and analogue information processing, *Nature 466*, 267-271.

41. El-Ali, J., Sorger, P. K., and Jensen, K. F. (2006) Cells on chips, *Nature 442*, 403-411.

42. Ducret, A., Maisonneuve, E., Notareschi, P., Grossi, A., Mignot, T., and Dukan, S. (2009) A microscope automated fluidic system to study bacterial processes in real time, *PloS one 4*, e7282.

43. Sun, P., Liu, Y., Sha, J., Zhang, Z., Tu, Q., Chen, P., and Wang, J. (2011) High-throughput microfluidic system for long-term bacterial colony monitoring and antibiotic testing in zero-flow environments, *Biosensors & bioelectronics 26*, 1993-1999.

44. Groisman, A., Lobo, C., Cho, H., Campbell, J. K., Dufour, Y. S., Stevens, A. M., and Levchenko, A. (2005) A microfluidic chemostat for experiments with bacterial and yeast cells, *Nature methods 2*, 685-689.

45. Chan, S. D., Luedke, G., Valer, M., Buhlmann, C., and Preckel, T. (2003) Cytometric analysis of protein expression and apoptosis in human primary cells with a novel microfluidic chip-based system, *Cytometry. Part A : the journal of the International Society for Analytical Cytology 55*, 119-125.

46. Huh, D., Gu, W., Kamotani, Y., Grotberg, J. B., and Takayama, S. (2005) Microfluidics for flow cytometric analysis of cells and particles, *Physiological measurement 26*, R73-98.

47. Simonnet, C., and Groisman, A. (2006) High-throughput and high-resolution flow cytometry in molded microfluidic devices, *Analytical chemistry 78*, 5653-5663.

48. Palkova, Z., Vachova, L., Valer, M., and Preckel, T. (2004) Single-cell analysis of yeast, mammalian cells, and fungal spores with a microfluidic pressure-driven chip-based system, *Cytometry. Part A : the journal of the International Society for Analytical Cytology 59*, 246-253.

49. Ehrlich, D. J., McKenna, B. K., Evans, J. G., Belkina, A. C., Denis, G. V., Sherr, D. H., and Cheung, M. C. (2011) Parallel imaging microfluidic cytometer, *Methods Cell Biol 102*, 49-75.

50. Perroud, T. D., Kaiser, J. N., Sy, J. C., Lane, T. W., Branda, C. S., Singh, A. K., and Patel, K. D. (2008) Microfluidic-based cell sorting of Francisella

tularensis infected macrophages using optical forces, *Analytical chemistry 80*, 6365-6372.

51. Fu, A. Y., Spence, C., Scherer, A., Arnold, F. H., and Quake, S. R. (1999) A microfabricated fluorescence-activated cell sorter, *Nature biotechnology 17*, 1109-1111.

52. Wang, M. M., Tu, E., Raymond, D. E., Yang, J. M., Zhang, H., Hagen, N., Dees, B., Mercer, E. M., Forster, A. H., Kariv, I., Marchand, P. J., and Butler, W. F. (2005) Microfluidic sorting of mammalian cells by optical force switching, *Nature biotechnology 23*, 83-87.

53. Taylor, R. J., Falconnet, D., Niemisto, A., Ramsey, S. A., Prinz, S., Shmulevich, I., Galitski, T., and Hansen, C. L. (2009) Dynamic analysis of MAPK signaling using a high-throughput microfluidic single-cell imaging platform, *Proceedings of the National Academy of Sciences of the United States of America 106*, 3758-3763.

54. Tay, S., Hughey, J. J., Lee, T. K., Lipniacki, T., Quake, S. R., and Covert, M. W. Single-cell NF-kappaB dynamics reveal digital activation and analogue information processing, *Nature 466*, 267-271.

55. Faley, S. L., Copland, M., Reboud, J., and Cooper, J. M. (2011) Cell chip array for microfluidic proteomics enabling rapid in situ assessment of intracellular protein phosphorylation, *Biomicrofluidics 5*, 24106.

56. Gossett, D. R., Weaver, W. M., Ahmed, N. S., and Di Carlo, D. (2011) Sequential array cytometry: multi-parameter imaging with a single fluorescent channel, *Annals of biomedical engineering 39*, 1328-1334.

57. Liu, P., Meagher, R. J., Light, Y. K., Yilmaz, S., Chakraborty, R., Arkin, A. P., Hazen, T. C., and Singh, A. K. (2011) Microfluidic fluorescence in situ hybridization and flow cytometry (muFlowFISH), *Lab on a chip 11*, 2673-2679.

58. Zhang, D. M., and Mao, B. L. (2003) [Relationships between LPS-tolerance and TLR4 as well as its signaling pathway], *Sheng Li Ke Xue Jin Zhan 34*, 277-279.

59. Parker, L. C., Whyte, M. K., Vogel, S. N., Dower, S. K., and Sabroe, I. (2004) Toll-like receptor (TLR)2 and TLR4 agonists regulate CCR expression in human monocytic cells, *J Immunol 172*, 4977-4986.

60. von Meyenburg, C., Hrupka, B. H., Arsenijevic, D., Schwartz, G. J., Landmann, R., and Langhans, W. (2004) Role for CD14, TLR2, and TLR4 in bacterial product-induced anorexia, *Am J Physiol Regul Integr Comp Physiol 287*, R298-305.

61. Romics, L., Jr., Dolganiuc, A., Kodys, K., Drechsler, Y., Oak, S., Velayudham, A., Mandrekar, P., and Szabo, G. (2004) Selective priming to Toll-like receptor 4 (TLR4), not TLR2, ligands by P. acnes involves up-regulation of MD-2 in mice, *Hepatology 40*, 555-564.

62. Hietaranta, A., Mustonen, H., Puolakkainen, P., Haapiainen, R., and Kemppainen, E. (2004) Proinflammatory effects of pancreatic elastase are mediated through TLR4 and NF-kappaB, *Biochem Biophys Res Commun 323*, 192-196.

63. Lehnardt, S., Lachance, C., Patrizi, S., Lefebvre, S., Follett, P. L., Jensen, F. E., Rosenberg, P. A., Volpe, J. J., and Vartanian, T. (2002) The toll-like receptor TLR4 is necessary for lipopolysaccharide-induced oligodendrocyte injury in the CNS, *J Neurosci 22*, 2478-2486.

64. Cheng, X., Irimia, D., Dixon, M., Ziperstein, J. C., Demirci, U., Zamir, L., Tompkins, R. G., Toner, M., and Rodriguez, W. R. (2007) A microchip approach for practical label-free CD4+ T-cell counting of HIV-infected subjects in resource-poor settings, *J Acquir Immune Defic Syndr 45*, 257-261.

65. Bernheiden, M., Heinrich, J. M., Minigo, G., Schutt, C., Stelter, F., Freeman, M., Golenbock, D., and Jack, R. S. (2001) LBP, CD14, TLR4 and the murine innate immune response to a peritoneal Salmonella infection, *J Endotoxin Res 7*, 447-450.

66. Kimoto, M., Nagasawa, K., and Miyake, K. (2003) Role of TLR4/MD-2 and RP105/MD-1 in innate recognition of lipopolysaccharide, *Scand J Infect Dis 35*, 568-572.

67. An, H., Yu, Y., Zhang, M., Xu, H., Qi, R., Yan, X., Liu, S., Wang, W., Guo, Z., Guo, J., Qin, Z., and Cao, X. (2002) Involvement of ERK, p38 and NF-kappaB signal transduction in regulation of TLR2, TLR4 and TLR9 gene expression induced by lipopolysaccharide in mouse dendritic cells, *Immunology 106*, 38-45.

68. Abkarian, M., Faivre, M., Horton, R., Smistrup, K., Best-Popescu, C. A., and Stone, H. A. (2008) Cellular-scale hydrodynamics, *Biomed Mater 3*, 034011.

69. Morrison, D. C., and Ryan, J. L. (1987) Endotoxins and disease mechanisms, *Annu Rev Med 38*, 417-432.

70. Tracey, K. J., Lowry, S. F., Fahey, T. J., 3rd, Albert, J. D., Fong, Y., Hesse, D., Beutler, B., Manogue, K. R., Calvano, S., Wei, H., and et al. (1987) Cachectin/tumor necrosis factor induces lethal shock and stress hormone responses in the dog, *Surg Gynecol Obstet 164*, 415-422.

71. Ulevitch, R. J., and Tobias, P. S. (1995) Receptor-dependent mechanisms of cell stimulation by bacterial endotoxin, *Annu Rev Immunol 13*, 437-457.

72. An, G. C., and Faeder, J. R. (2009) Detailed qualitative dynamic knowledge representation using a BioNetGen model of TLR-4 signaling and preconditioning, *Mathematical Biosciences 217*, 53-63.

73. An, G. (2009) A model of TLR4 signaling and tolerance using a qualitative, particle-event-based method: Introduction of spatially configured stochastic reaction chambers (SCSRC), *Mathematical Biosciences 217*, 43-52.

74. Blinov, M. L., Faeder, J. R., Goldstein, B., and Hlavacek, W. S. (2004) BioNetGen: software for rule-based modeling of signal transduction based on the interactions of molecular domains, *Bioinformatics 20*, 3289-3291.

75. Shin, H. J., Lee, H., Park, J. D., Hyun, H. C., Sohn, H. O., Lee, D. W., and Kim, Y. S. (2007) Kinetics of binding of LPS to recombinant CD14, TLR4, and MD-2 proteins, *Mol Cells 24*, 119-124.

76. Thomas, C. J., Kapoor, M., Sharma, S., Bausinger, H., Zyilan, U., Lipsker, D., Hanau, D., and Surolia, A. (2002) Evidence of a trimolecular complex

involving LPS, LPS binding protein and soluble CD14 as an effector of LPS response, *FEBS Lett 531*, 184-188.

77. Krutzik, P. O., and Nolan, G. P. (2003) Intracellular phospho-protein staining techniques for flow cytometry: monitoring single cell signaling events, *Cytometry. Part A : the journal of the International Society for Analytical Cytology 55*, 61-70.

78. Torres, C. R., and Hart, G. W. (1984) Topography and polypeptide distribution of terminal N-acetylglucosamine residues on the surfaces of intact lymphocytes. Evidence for O-linked GlcNAc, *The Journal of biological chemistry 259*, 3308-3317.

79. Hart, G. W., and Akimoto, Y. (2009) The O-GlcNAc Modification, in *Essentials of Glycobiology* (Varki, A., Cummings, R. D., Esko, J. D., Freeze, H. H., Stanley, P., Bertozzi, C. R., Hart, G. W., and Etzler, M. E., Eds.) 2nd ed., Cold Spring Harbor (NY).

80. Zachara, N. E. (2009) Detection and analysis of (O-linked beta-N-acetylglucosamine)-modified proteins, *Methods Mol Biol 464*, 227-254.

81. Comer, F. I., and Hart, G. W. (2000) O-Glycosylation of nuclear and cytosolic proteins. Dynamic interplay between O-GlcNAc and O-phosphate, *The Journal of biological chemistry 275*, 29179-29182.

82. Holt, G. D., Haltiwanger, R. S., Torres, C. R., and Hart, G. W. (1987) Erythrocytes contain cytoplasmic glycoproteins. O-linked GlcNAc on Band 4.1, *The Journal of biological chemistry 262*, 14847-14850.

83. Lazarus, B. D., Love, D. C., and Hanover, J. A. (2006) Recombinant O-GlcNAc transferase isoforms: identification of O-GlcNAcase, yes tyrosine kinase, and tau as isoform-specific substrates, *Glycobiology 16*, 415-421.

84. Gao, Y., Wells, L., Comer, F. I., Parker, G. J., and Hart, G. W. (2001) Dynamic O-glycosylation of nuclear and cytosolic proteins: cloning and characterization of a neutral, cytosolic beta-N-acetylglucosaminidase from human brain, *The Journal of biological chemistry 276*, 9838-9845.

85. Golks, A., and Guerini, D. (2008) The O-linked N-acetylglucosamine modification in cellular signalling and the immune system. 'Protein modifications: beyond the usual suspects' review series, *EMBO reports 9*, 748-753.

86. Kneass, Z. T., and Marchase, R. B. (2005) Protein O-GlcNAc modulates motility-associated signaling intermediates in neutrophils, *The Journal of biological chemistry 280*, 14579-14585.

87. Kearse, K. P., and Hart, G. W. (1991) Lymphocyte activation induces rapid changes in nuclear and cytoplasmic glycoproteins, *Proceedings of the National Academy of Sciences of the United States of America 88*, 1701-1705.

88. Golks, A., Tran, T. T., Goetschy, J. F., and Guerini, D. (2007) Requirement for O-linked N-acetylglucosaminyltransferase in lymphocytes activation, *The EMBO journal 26*, 4368-4379.

89. Zachara, N. E., Vosseller, K., and Hart, G. W. (2011) Detection and analysis of proteins modified by O-linked N-acetylglucosamine, *Current protocols in*

molecular biology / edited by Frederick M. Ausubel ... [et al.] Chapter 17, Unit 17 16.

90. Vocadlo, D. J., Hang, H. C., Kim, E. J., Hanover, J. A., and Bertozzi, C. R. (2003) A chemical approach for identifying O-GlcNAc-modified proteins in cells, *Proceedings of the National Academy of Sciences of the United States of America 100*, 9116-9121.

91. Soderberg, O., Gullberg, M., Jarvius, M., Ridderstrale, K., Leuchowius, K. J., Jarvius, J., Wester, K., Hydbring, P., Bahram, F., Larsson, L. G., and Landegren, U. (2006) Direct observation of individual endogenous protein complexes in situ by proximity ligation, *Nature methods 3*, 995-1000.

92. Yuzwa, S. A., Macauley, M. S., Heinonen, J. E., Shan, X., Dennis, R. J., He, Y., Whitworth, G. E., Stubbs, K. A., McEachern, E. J., Davies, G. J., and Vocadlo, D. J. (2008) A potent mechanism-inspired O-GlcNAcase inhibitor that blocks phosphorylation of tau in vivo, *Nature chemical biology 4*, 483-490.

93. Wu, M., Perroud, TD., Srivastava N., C.S. Branda , K. Sale, B.D. Carson, K. D. Patel, S.S. Branda, Anup K. Singh. (2012) Microfluidically-unified cell culture, sample preparation, imaging and flow cytometry for measurement of cell signaling pathways with single cell resolution, *Lab Chip, DOI:10.1039/C2LC40344G*.

94. Landgraf, P., Rusu, M., Sheridan, R., Sewer, A., Iovino, N., Aravin, A., Pfeffer, S., Rice, A., Kamphorst, A. O., Landthaler, M., Lin, C., Socci, N. D., Hermida, L., Fulci, V., Chiaretti, S., Foa, R., Schliwka, J., Fuchs, U., Novosel,

A., Muller, R. U., Schermer, B., Bissels, U., Inman, J., Phan, Q., Chien, M., Weir, D. B., Choksi, R., De Vita, G., Frezzetti, D., Trompeter, H. I., Hornung, V., Teng, G., Hartmann, G., Palkovits, M., Di Lauro, R., Wernet, P., Macino, G., Rogler, C. E., Nagle, J. W., Ju, J., Papavasiliou, F. N., Benzing, T., Lichter, P., Tam, W., Brownstein, M. J., Bosio, A., Borkhardt, A., Russo, J. J., Sander, C., Zavolan, M., and Tuschl, T. (2007) A mammalian microRNA expression atlas based on small RNA library sequencing, *Cell 129*, 1401-1414.

95. Baltimore, D., Boldin, M. P., O'Connell, R. M., Rao, D. S., and Taganov, K. D. (2008) MicroRNAs: new regulators of immune cell development and function, *Nature immunology 9*, 839-845.

96. Lodish, H. F., Zhou, B., Liu, G., and Chen, C. Z. (2008) Micromanagement of the immune system by microRNAs, *Nature reviews. Immunology 8*, 120-130.

97. Krutzfeldt, J., and Stoffel, M. (2006) MicroRNAs: a new class of regulatory genes affecting metabolism, *Cell metabolism 4*, 9-12.

98. Griffiths-Jones, S. (2010) miRBase: microRNA sequences and annotation, *Current protocols in bioinformatics / editoral board, Andreas D. Baxevanis ... [et al.] Chapter 12*, Unit 12 19 11-10.

99. O'Connell, R. M., Rao, D. S., Chaudhuri, A. A., and Baltimore, D. (2010) Physiological and pathological roles for microRNAs in the immune system, *Nature reviews. Immunology 10*, 111-122.

100. Rosenbauer, F., and Tenen, D. G. (2007) Transcription factors in myeloid development: balancing differentiation with transformation, *Nature reviews. Immunology 7*, 105-117.

101. Wu, H., Neilson, J. R., Kumar, P., Manocha, M., Shankar, P., Sharp, P. A., and Manjunath, N. (2007) miRNA profiling of naive, effector and memory CD8 T cells, *PloS one 2*, e1020.

102. Tan, L. P., Wang, M., Robertus, J. L., Schakel, R. N., Gibcus, J. H., Diepstra, A., Harms, G., Peh, S. C., Reijmers, R. M., Pals, S. T., Kroesen, B. J., Kluin, P. M., Poppema, S., and van den Berg, A. (2009) miRNA profiling of B-cell subsets: specific miRNA profile for germinal center B cells with variation between centroblasts and centrocytes, *Laboratory investigation; a journal of technical methods and pathology 89*, 708-716.

103. Martinez-Nunez, R. T., Louafi, F., Friedmann, P. S., and Sanchez-Elsner, T. (2009) MicroRNA-155 modulates the pathogen binding ability of dendritic cells (DCs) by down-regulation of DC-specific intercellular adhesion molecule-3 grabbing non-integrin (DC-SIGN), *The Journal of biological chemistry 284*, 16334-16342.

104. Hashimi, S. T., Fulcher, J. A., Chang, M. H., Gov, L., Wang, S., and Lee, B. (2009) MicroRNA profiling identifies miR-34a and miR-21 and their target genes JAG1 and WNT1 in the coordinate regulation of dendritic cell differentiation, *Blood 114*, 404-414.

105. Pena, J. T., Sohn-Lee, C., Rouhanifard, S. H., Ludwig, J., Hafner, M., Mihailovic, A., Lim, C., Holoch, D., Berninger, P., Zavolan, M., and Tuschl, T. (2009) miRNA in situ hybridization in formaldehyde and EDC-fixed tissues, *Nature methods 6*, 139-141.

106. de Planell-Saguer, M., Rodicio, M. C., and Mourelatos, Z. (2010) Rapid in situ codetection of noncoding RNAs and proteins in cells and formalin-fixed paraffin-embedded tissue sections without protease treatment, *Nature protocols 5*, 1061-1073.

107. Speel, E. J., Hopman, A. H., and Komminoth, P. (2006) Tyramide signal amplification for DNA and mRNA in situ hybridization, *Methods Mol Biol 326*, 33-60.

108. O'Connell, R. M., Taganov, K. D., Boldin, M. P., Cheng, G., and Baltimore, D. (2007) MicroRNA-155 is induced during the macrophage inflammatory response, *Proceedings of the National Academy of Sciences of the United States of America 104*, 1604-1609.

109. Thai, T. H., Calado, D. P., Casola, S., Ansel, K. M., Xiao, C., Xue, Y., Murphy, A., Frendewey, D., Valenzuela, D., Kutok, J. L., Schmidt-Supprian, M., Rajewsky, N., Yancopoulos, G., Rao, A., and Rajewsky, K. (2007) Regulation of the germinal center response by microRNA-155, *Science 316*, 604-608.

110. Lu, L. F., Thai, T. H., Calado, D. P., Chaudhry, A., Kubo, M., Tanaka, K., Loeb, G. B., Lee, H., Yoshimura, A., Rajewsky, K., and Rudensky, A. Y. (2009) Foxp3-dependent microRNA155 confers competitive fitness to regulatory T cells by targeting SOCS1 protein, *Immunity 30*, 80-91.

111. Ceppi, M., Pereira, P. M., Dunand-Sauthier, I., Barras, E., Reith, W., Santos, M. A., and Pierre, P. (2009) MicroRNA-155 modulates the interleukin-1 signaling pathway in activated human monocyte-derived dendritic cells,

Proceedings of the National Academy of Sciences of the United States of America 106, 2735-2740.

112. Lu, C., Huang, X., Zhang, X., Roensch, K., Cao, Q., Nakayama, K. I., Blazar, B. R., Zeng, Y., and Zhou, X. (2011) miR-221 and miR-155 regulate human dendritic cell development, apoptosis, and IL-12 production through targeting of p27kip1, KPC1, and SOCS-1, *Blood 117*, 4293-4303.

113. O'Connell, R. M., Chaudhuri, A. A., Rao, D. S., and Baltimore, D. (2009) Inositol phosphatase SHIP1 is a primary target of miR-155, *Proceedings of the National Academy of Sciences of the United States of America 106*, 7113-7118.

114. Murata, K., Yoshitomi, H., Tanida, S., Ishikawa, M., Nishitani, K., Ito, H., and Nakamura, T. (2010) Plasma and synovial fluid microRNAs as potential biomarkers of rheumatoid arthritis and osteoarthritis, *Arthritis research & therapy 12*, R86.

115. Paraskevi, A., Theodoropoulos, G., Papaconstantinou, I., Mantzaris, G., Nikiteas, N., and Gazouli, M. (2012) Circulating MicroRNA in inflammatory bowel disease, *Journal of Crohn's & colitis*.

116. Willimott, S., and Wagner, S. D. (2012) miR-125b and miR-155 contribute to BCL2 repression and proliferation in response to CD40 ligand (CD154) in human leukemic B-cells, *The Journal of biological chemistry 287*, 2608-2617.

117. Garzon, R., Marcucci, G., and Croce, C. M. (2010) Targeting microRNAs in cancer: rationale, strategies and challenges, *Nature reviews. Drug discovery 9*, 775-789.

118. Weiss, A., Wiskocil, R. L., and Stobo, J. D. (1984) The role of T3 surface molecules in the activation of human T cells: a two-stimulus requirement for IL 2 production reflects events occurring at a pre-translational level, *J Immunol 133*, 123-128.

119. Baerlocher, G. M., Vulto, I., de Jong, G., and Lansdorp, P. M. (2006) Flow cytometry and FISH to measure the average length of telomeres (flow FISH), *Nature protocols 1*, 2365-2376.

120. Robertson, K. L., and Thach, D. C. (2009) LNA flow-FISH: a flow cytometry-fluorescence in situ hybridization method to detect messenger RNA using locked nucleic acid probes, *Analytical biochemistry 390*, 109-114.

121. Nielsen, B. S. (2012) MicroRNA in situ hybridization, *Methods Mol Biol 822*, 67-84.

122. Andreasen, D., Fog, J. U., Biggs, W., Salomon, J., Dahslveen, I. K., Baker, A., and Mouritzen, P. (2010) Improved microRNA quantification in total RNA from clinical samples, *Methods 50*, S6-9.

123. Yiemwattana, I., Ngoenkam, J., Paensuwan, P., Kriangkrai, R., Chuenjitkuntaworn, B., and Pongcharoen, S. (2012) Essential role of the adaptor protein Nck1 in Jurkat T cell activation and function, *Clinical and experimental immunology 167*, 99-107.

124. Du, T. T., Fu, Y. F., Dong, M., Wang, L., Fan, H. B., Chen, Y., Jin, Y., Chen, S. J., Chen, Z., Deng, M., Huang, Q. H., and Liu, T. X. (2009) Experimental validation and complexity of miRNA-mRNA target interaction during

zebrafish primitive erythropoiesis, *Biochem Biophys Res Commun 381*, 688-693.